HHS Public Access

Author manuscript

Sci Transl Med. Author manuscript; available in PMC 2022 September 15.

Published in final edited form as:

Sci Transl Med. 2021 June 30; 13(600): . doi:10.1126/scitranslmed.abd6892.

Gene therapy knockdown of Hippo signaling induces cardiomyocyte renewal in pigs after myocardial infarction

Shijie Liu[1], **Ke Li**[1], **Leonardo Wagner Florencio**[1], **Li Tang**[2], **Todd R. Heallen**[1], **John P. Leach**[3,†], **Yidan Wang**[1], **Francisco Grisanti**[2], **James T. Willerson**[1,‡], **Emerson C. Perin**[1], **Sui Zhang**[1], **James F. Martin**[1,2,4,*]

[1]Texas Heart Institute, Houston, TX, USA

[2]Department of Molecular Physiology and Biophysics, Baylor College of Medicine, Houston, TX, USA

[3]Department of Medicine, Department of Cell and Developmental Biology, University of Pennsylvania Perelman School of Medicine, Philadelphia, PA, USA

[4]Center for Organ Repair and Renewal and Cardiovascular Research Institute, Baylor College of Medicine, Houston, TX, USA

Abstract

Human heart failure, a leading cause of death worldwide, is a prominent example of a chronic disease that may result from poor cell renewal. The Hippo signaling pathway is an inhibitory kinase cascade that represses adult heart muscle cell (cardiomyocyte) proliferation and renewal after myocardial infarction in genetically modified mice. Here, we investigated an adeno-associated virus 9 (AAV9)–based gene therapy to locally knock down the Hippo pathway gene Salvador (*Sav*) in border zone cardiomyocytes in a pig model of ischemia/reperfusion-induced myocardial infarction. Two weeks after myocardial infarction, when pigs had left ventricular systolic dysfunction, we administered AAV9-*Sav*–short hairpin RNA (shRNA) or a control AAV9 viral vector carrying green fluorescent protein (GFP) directly into border zone cardiomyocytes via catheter-mediated subendocardial injection. Three months after injection, pig hearts treated

*Corresponding author. jfmartin@bcm.edu.
†Present Address: Yap Therapeutics Inc., 2450 Holcombe Blvd., Suite BCM A, Houston, TX, USA.
‡Deceased.

Author contributions: S.L., J.T.W., S.Z., and J.F.M. designed the study. K.L., L.W.F., L.T., and E.C.P. conducted surgery and echocardiography. S.L., T.R.H., and Y.W. conducted the immunofluorescence staining and image analysis. L.T. and F G. performed machine learning analysis. S.L. and J.P.L. conducted statistical analysis. S.L., S.Z., and J.F.M wrote the manuscript. J.F.M., S.L., S.Z., T.R.H., E.C.P., and J.T.W. reviewed and edited the manuscript.

SUPPLEMENTARY MATERIALS

stm.sciencemag.org/cgi/content/full/13/600/eabd6892/DC1

Tables S1 to S6

Data file S1

Movies S1 to S6

View/request a protocol for this paper from Bio-protocol.

Competing interests: J.F.M. is a cofounder of and owns shares in Yap Therapeutics. J.F.M., T.R.H., and J.P.L. are coinventors on the following patents associated with this study: patent no. US20200206327A1 entitled “Hippo pathway deficiency reverses systolic heart failure post-infarction”, patent no. 15/642200.PCT/US2014/069349 101191411 entitled “Hippo and dystrophin complex signaling in cardiomyocyte renewal”, and patent no. 15/102593.PCT/US2014/069349 9732345 entitled “Hippo and dystrophin complex signaling in cardiomyocyte renewal.”

with a high dose of AAV9-*Sav*-shRNA exhibited a 14.3% improvement in ejection fraction (a measure of left ventricular systolic function), evidence of cardiomyocyte division, and reduced scar sizes compared to pigs receiving AAV9-GFP. AAV9-*Sav*-shRNA–treated pig hearts also displayed increased capillary density and reduced cardiomyocyte ploidy. AAV9-*Sav*-shRNA gene therapy was well tolerated and did not induce mortality. In addition, liver and lung pathology revealed no tumor formation. Local delivery of AAV9-*Sav*-shRNA gene therapy to border zone cardiomyocytes in pig hearts after myocardial infarction resulted in tissue renewal and improved function and may have utility in treating heart failure.

INTRODUCTION

After myocardial infarction in humans and other large animals, millions of cardiomyocytes fail to regenerate and die (1). After myocardial infarction–induced tissue damage, scar formation together with the loss of cardiomyocytes impairs contractile function and leads to pathological remodeling and heart failure (2). The long-lived and vanishingly small renewal capacity of adult cardiomyocytes contributes to the clinical intractability of heart failure (3). Human cardiomyocytes renew at a rate of about only 1% per year in young humans, as found in carbon isotope studies in postmortem cardiomyocyte nuclei (4). Mice also have extremely low rates of cardiomyocyte renewal (5, 6).

Neonatal mouse and pig hearts have the capacity to regenerate during a brief window of time after birth (7–9). There is also anecdotal evidence that the human heart can regenerate postnatally (10). Studies of mouse neonatal hearts revealed that new cardiomyocytes are derived from preexisting cardiomyocytes, suggesting that adult cardiomyocytes have the potential to be manipulated directly to regenerate the heart (11). Experiments in genetically modified mouse models support the hypothesis that heart disease can be treated by the direct manipulation of endogenous cardiomyocyte genes to induce a renewable cell state (12–14).

Although studies in mice have advanced our knowledge of cardiomyocyte and tissue renewal more broadly, how these insights will lead to therapies for chronic, untreatable human diseases such as heart failure remains unclear. Recent work with untargeted gain-of-function approaches that modulate large groups of cardiomyocytes has suggested that acutely inducing too much cardiomyocyte proliferation in mouse and pig cardiomyocytes can lead to their demise (15–17). An alternative approach, which we describe here, is to use catheter delivery technologies to specifically inject border zone cardiomyocytes with a gene therapy viral vector in a localized fashion (18). In addition to more accurately delivering the viral vector to cells of interest, catheter-based gene therapy allows for a reduction in viral dose on a per-kilogram basis.

The Hippo signaling pathway is activated in the heart in response to physiological inputs such as changes in extracellular matrix composition or mechanical signaling and is maladaptively up-regulated in human heart failure (12, 19). Core Hippo signaling pathway components, including the Mst kinases and the adaptor *Sav*, phosphorylate Lats kinases, which subsequently phosphorylate and inhibit the downstream transcription cofactors Yap and Taz. When Hippo pathway activity is low, Yap and Taz enter the nucleus, where they cooperate with Tead family transcription factors to activate target

genes. In adult cardiomyocytes, high Yap expression produced via transgene expression induces the transition of cells to a more fetal-like, renewable state by changing genome-wide chromatin accessibility (17). Yap-Tead target genes in cardiomyocytes include many genes that promote cell cycle progression, including multiple cyclin genes and genes that promote cytoskeletal remodeling and protrusion formation in border zone cardiomyocytes (20). Because *Sav* encodes an adaptor rather than a kinase, *Sav* loss of function moderately inhibits Hippo signaling, which is desirable for human cardiomyocyte renewal therapy (21). Moreover, because there is a single *Sav* gene in mammalian genomes, it is an attractive target for therapy. Mild Hippo pathway inhibition via *Sav* knockdown is a viable strategy to safely treat human heart failure, as has been suggested by studies in mice (12). Although mouse studies are valuable, they have limitations for translational studies because of the distinctly different cardiovascular anatomy and physiology between rodents and humans. In addition to obvious differences in size, heart rates are much faster in rodents (300 to 840 beats/min in mice and 330 to 480 beats/min in rats) than in humans (80 to 100 beats/min) (22, 23). In contrast, pig hearts share many similarities with human hearts, both in the steady state and after myocardial infarction (22, 23). For example, pig and human hearts have similar contractile indices, as determined by cardiac catheterization measurements (24, 25). Furthermore, pig and human cardiomyocytes share many characteristics in excitation-contraction coupling. Similar to human cardiomyocytes, pig cardiomyocytes predominantly express β-myosin heavy chain, and, similar to the human heart, both stiff N2B and compliant N2BA titin isoforms are expressed in pig myocardium (24). Pigs also share similar regional cardiac hemodynamic features with humans (26). In diseased pig and human hearts, altered myofilament function is seen after myocardial infarction (23), and both pig and human hearts show reduced contractility after myocardial infarction, which is caused by alterations in Ca^{2+} handling (23). Reduced SERCA2a expression has been reported in both species (23). Increased Ca^{2+} sensitivity is also a common feature in pig and human hearts after myocardial infarction (25), and the two species share hemodynamic similarities in heart failure secondary to increased afterload (27). In this study, we used a pig model of ischemic heart disease to investigate adeno-associated virus 9 (AAV9) gene therapy, delivered via a catheter-based NOGA electromechanical mapping system directly to border zone cardiomyocytes, to knock down *Sav* and induce endogenous cardiomyocyte renewal after myocardial infarction (28).

RESULTS

Viral vector delivery of *Sav*-shRNA induces Hippo pathway deficiency in adult pig cardiomyocytes

Our first objective was to determine whether an AAV9 viral vector encoding short hairpin RNAs (shRNAs) against *Sav* (AAV9-*Sav*-shRNA) could improve cardiomyocyte renewal rates in uninjured pig hearts. Using a Myostar catheter and NOGA electromechanical mapping, we delivered AAV9-*Sav*-shRNA (fig. S1A) directly into the myocardial wall of 3-month-old pigs via subendocardial injection (Table 1). NOGA electromechanical mapping provides an accurate three-dimensional visualization of infarcted border zone cardiomyocyte regions (18). The AAV9-*Sav*-shRNA viral vector encoded a green fluorescent protein (GFP)

reporter to visualize infected cardiomyocytes and three shRNAs against *Sav* (12), whereas the control viral vector carried the GFP cassette alone (AAV9-GFP).

We injected a total of 1×10^{13} viral genome copies of AAV9-*Sav*-shRNA, referred to as low dose, into the cardiac apex of pigs ($n = 6$ per group) using the NOGA system, which is equivalent to about 3.4×10^{11} viral genome copies per kilogram (fig. S1B). One month after viral injection (pig age at euthanasia, 120 ± 12 days), pig hearts were harvested and cardiac sections containing viral injection sites (determined by NOGA mapping) were analyzed (fig. S1, C and D). Immunofluorescence staining for GFP to determine the efficiency of viral infection revealed a patchy distribution of GFP-expressing cardiomyocytes surrounding the injection sites (Fig. 1A and fig. S2, A and B). Tiled imaging of large areas of myocardium revealed that the surface area of GFP-positive myocardium was about 20 mm^2 per section and that cardiomyocyte-restricted viral infection was localized in close proximity to injection sites (Fig. 1A and fig. S2B).

To validate Hippo pathway knockdown by AAV9-*Sav*-shRNA injection, we examined the subcellular localization of Yap, which translocates into the nucleus when Hippo signaling is reduced (19). Immunofluorescence staining revealed that Yap nuclear localization was increased in cardiomyocytes from AAV9-*Sav*-shRNA–injected hearts compared with those from AAV9-GFP–injected hearts ($P < 0.0001$, GFP-positive area; Fig. 1, B and C). A portion of GFP-negative cardiomyocytes in AAV9-*Sav*-shRNA–injected hearts also had increased nuclear Yap, suggesting that signaling between cardiomyocytes may promote Yap nuclear localization or that GFP expression was diluted after cardiomyocyte division ($P = 0.0051$, GFP-negative area; Fig. 1, B and C). Our findings indicate that low-dose, local injection of AAV9-*Sav*-shRNA into pig myocardium reduced Hippo pathway activity in uninjured adult pig cardiomyocytes.

Targeted AAV9-*Sav*-shRNA gene therapy induces cardiomyocyte proliferation in uninjured pig hearts

Pig cardiomyocytes are multinucleated as a result of extensive endoreplication that ceases at about 6 months of age (8, 29). Because the pigs in our study were about 3 months of age at the time of injection (Table 1), we expected to observe background cell cycle activity without cardiomyocyte cell division in control pig hearts. 5-Ethynyl-2′-deoxyuridine (EdU), which stably incorporates into DNA during S phase, acts as a lineage tracer and is retained by cardiomyocyte daughter cells after cardiomyocytes divide. Therefore, we used EdU incorporation assays to identify EdU-positive cardiomyocytes located side by side with adjoining plasma membranes, as a method for identifying cardiomyocytes that had divided.

To visualize and trace pig cardiomyocytes that had entered S phase, we injected three doses of EdU intravenously at 9- to 10-day intervals after viral vector injections and harvested pig hearts 1 month after viral injection (pig age at euthanasia, 120 ± 12 days) (Fig. 2A). Counting of a large number (>70,000) of cardiomyocytes using tiled image analysis combined with machine learning revealed that a trace amount of cardiomyocytes in AAV9-GFP–injected pig hearts entered S phase due to endoreplication (Fig. 2, B and C, and fig. S3) (29–31). The number of EdU-positive cardiomyocytes was about threefold higher in AAV9-*Sav*-shRNA–injected pig hearts than in control hearts ($P =$

0.0095, GFP-positive areas; Fig. 2, B and C). Furthermore, GFP-negative cardiomyocytes exhibited S phase entry in AAV9-*Sav*-shRNA–injected hearts, suggesting that cell cycle entry was also induced in cardiomyocytes located distally from the injection site, perhaps due to a paracrine mechanism or dilution of GFP after cardiomyocyte division (P = 0.004, GFP-negative area; Fig. 2C). In control AAV9-GFP–injected hearts, no paired EdU-positive cardiomyocytes were located side by side to indicate cardiomyocyte division. In contrast, AAV9-*Sav*-shRNA–injected hearts displayed paired EdU-positive cardiomyocytes, supporting the hypothesis that cardiomyocytes of AAV9-*Sav*-shRNA–injected hearts divided into two daughter cardiomyocytes (P = 0.0334 and P = 0.0496 for GFP-positive and GFP-negative areas, respectively; Fig. 2, B and D).

We used machine learning counting of tiled images to globally quantify all EdU-positive cardiomyocytes, both GFP positive and GFP negative, in proximity to the injection sites. In AAV9-GFP–injected control pig hearts, about 0.20 ± 0.05% (mean ± SEM) of the cardiomyocytes were EdU positive [median, 0.13 (interquartile range, 0.16); 73,008 cardiomyocytes], whereas in AAV9-*Sav*-shRNA–injected pig hearts, 0.80 ± 0.14% of cardiomyocytes were EdU positive [median, 0.63 (interquartile range, 0.91); 113,029 cardiomyocytes] (P = 0.0247; Fig. 2E). Moreover, immunofluorescence staining for phosphorylated histone H3 (pHH3), a marker of M phase, revealed pHH3-positive cardiomyocytes in pig hearts injected with AAV9-GFP or AAV9-*Sav*-shRNA (Fig. 2F). We observed about twice as many pHH3-positive cardiomyocytes in AAV9-*Sav*-shRNA–injected hearts than in AAV9-GFP–injected control hearts (P = 0.0159; Fig. 2, F and G). In addition, in AAV9-*Sav*-shRNA–injected hearts, we observed clusters of EdU-positive cardiomyocytes in proximity to pHH3-positive cardiomyocytes, suggesting that cardiomyocytes in low-dose AAV9-*Sav*-shRNA–injected hearts divided (P = 0.0079; Fig. 2, F and H). Within the clusters, some pHH3-positive cardiomyocytes were EdU negative. Given that EdU is a lineage tracer, pHH3-positive/EdU-negative cardiomyocytes are unlikely to share a simple mother-daughter lineage relationship. Although more studies are required to understand this observation, the pHH3-positive/EdU-negative cardiomyocytes, which missed the short window of EdU pulse labeling, may represent an effect of AAV9-*Sav*-shRNA–infected cardiomyocytes promoting cell cycle entry of surrounding cardiomyocytes in a nonautonomous fashion, as has been observed in a Yap5SA gain-of-function mouse model (17).

Viral vector delivery of *Sav*-shRNA improves systolic function in a pig model of myocardial infarction

To determine whether AAV9-*Sav*-shRNA promotes heart regeneration after myocardial infarction, we used an angioplasty balloon to induce myocardial infarction via ischemia/reperfusion (I/R) injury in ~3-month-old pig hearts (pig age, 89 ± 11 days) by transiently occluding the left anterior descending artery for 90 min, followed by reperfusion (Fig. 3A). For the experiments in the myocardial infarction model, we used two different doses of AAV9-*Sav*-shRNA viral vector. Two weeks after myocardial infarction, echocardiography revealed a reduction in left ventricular ejection fraction to below 40% in all groups [AAV9-GFP control, ejection fraction: 36.2 ± 2.0%; low-dose AAV9-*Sav*-shRNA, ejection fraction: 36.5 ± 1.7%; high-dose AAV9-*Sav*-shRNA, ejection fraction: 33.7 ± 2.9% (mean

± SEM)] (Fig. 3B and fig. S4A), indicating efficient reduction in heart function. Moreover, transmural scars in the anterior wall were prominent, indicating that myocardial infarction was successfully induced by the I/R procedure (fig. S4, B and C). We injected AAV9-GFP or AAV9-*Sav*-shRNA into border zone myocardium using NOGA mapping to localize the injection sites (fig. S4D), and echocardiography was performed at 20, 40, 60, and 90 days after virus injections to longitudinally monitor heart function in each pig (Fig. 3A).

The longitudinal analyses of AAV9-GFP–injected pig hearts revealed that left ventricular function steadily worsened, consistent with progressive pathologic remodeling. In contrast, in AAV9-*Sav*-shRNA–injected hearts, left ventricular function progressively improved over time (Fig. 3, B to F, fig. S5A, and movies S1 to S6). In AAV9-GFP–injected hearts, ejection fraction dropped an additional 6.3 ± 1.9% during the 3-month follow-up period (pig age at euthanasia, 190 ± 12 days) (*P* values, Fig. 3, C to F and data file S1), whereas in the low-dose AAV9-*Sav*-shRNA–injected hearts, the ejection fraction increased by 4.1 ± 2% (1×10^{13} viral genome copies per experimental group) (Fig. 3, C to F). Three pigs, administered a high dose of AAV9-*Sav*-shRNA (4×10^{13} viral genome copies), exhibited a robust improvement in ejection fraction (8.0 ± 0.5%) at day 104 after myocardial infarction compared with day 14 (Fig. 3, C to F). The difference in ejection fraction between high and low viral vector doses failed to show a statistical difference, most likely because of the limited number of pigs in the high-dose group (Fig. 3, E and F). AAV9-GFP control-treated pigs exhibited an increase in absolute heart weight and heart weight–to–body weight (HW/BW) ratio compared with AAV9-*Sav*-shRNA–treated pigs, suggesting that control pigs underwent cardiac hypertrophy. Increased HW/BW ratio may also represent immune cell infiltration and increased extracellular matrix deposition with more fibrosis ($P = 0.0041$; fig. S5B).

AAV9-*Sav*-shRNA treatment improved left ventricular systolic function over time with only a marginal effect on diastolic function, indicating that improved ejection fraction was primarily due to restored left ventricular systolic function ($P = 0.0283$ for Fig. 3G; $P = 0.0036$ for Fig. 3H; figs. S5, C and D). Consistent with this, compared with AAV9-GFP–injected hearts, AAV9-*Sav*-shRNA–injected hearts showed improved stroke volume ($P = 0.0041$ for Fig. 3I; $P = 0.0096$ for fig. S5E). Three months after virus injections, all pigs were euthanized (pig age, 190 ± 12 days), and hearts were carefully analyzed. Transmural scars were observed in all hearts and were smaller in AAV9-*Sav*-shRNA–injected hearts than in control hearts (Fig. 3, J to L, and Table 2). After sectioning ventricles into seven slices, we measured the infarct area in each slice and observed reduced scarring in AAV9-*Sav*-shRNA–injected hearts compared with control hearts ($P = 0.0346$; Fig. 3, K and L, and figs. S6 and S7). Together, these data indicate that AAV9-*Sav*-shRNA treatment improved left ventricular systolic heart function and reduced scar formation in a pig model of myocardial infarction.

Blood test results revealed normal white and red blood cell counts, as well as normal liver and kidney function 45 days after viral injection (pig age, 145 ± 12 days) (Table 3). When we closely examined liver and lung tissues 3 months after viral vector injection, no tumors were observed, indicating that localized injection of AAV9-*Sav*-shRNA was safely tolerated (see Materials and Methods and pathology report in tables S1 to S3).

Viral vector delivery of *Sav*-shRNA increases cardiomyocyte cell cycle entry and division in pig hearts after myocardial infarction

We examined cardiomyocyte cell cycle activity in pig hearts 3 months after myocardial infarction. Immunofluorescence staining for GFP in cardiomyocytes indicated that AAV9-*Sav*-shRNA expression persisted for 3 months after viral injection (pig age at euthanasia, 190 ± 12 days) (fig. S8). Immunofluorescence staining further revealed that the nuclear Yap index in cardiomyocytes of AAV9-*Sav*-shRNA–injected hearts was higher than that of control hearts ($P = 0.0075$ and $P < 0.0001$ for GFP-negative and GFP-positive areas, respectively; fig. S9, A and B). The nuclear Yap index in cardiomyocytes residing in GFP-negative areas was also higher in AAV9-*Sav*-shRNA–injected hearts than in control hearts, suggesting a paracrine mechanism or dilution of GFP after cardiomyocyte division.

After seven injections of EdU performed at 10- to 20-day intervals beginning 10 days after viral injection (Fig. 3A), image analysis and machine learning counting revealed that the number of EdU-labeled cardiomyocytes had more than doubled in hearts injected with low-dose AAV9-*Sav*-shRNA and tripled in hearts injected with high-dose AAV9-*Sav*-shRNA compared with controls ($P = 0.0124$ and $P < 0.0001$ for GFP control versus low-dose or high-dose *Sav*-shRNA, respectively; Fig. 4, A and B). Tiled image analysis revealed clusters of EdU-positive cardiomyocytes distributed over multiple areas of AAV9-*Sav*-shRNA–injected hearts, including paired EdU-positive cardiomyocytes, suggesting that cardiomyocytes had divided (Fig. 4, C and D). Paired EdU-positive cardiomyocytes were infrequently observed in control AAV9-GFP–injected hearts, most likely as a result of a systematic error in imaging EdU-positive cardiomyocytes on sections after myocardial infarction ($P = 0.0448$ and $P = 0.0044$ between GFP control compared to low-dose or high-dose *Sav*-shRNA, respectively; Fig. 4D) (32). We also observed a higher number of pHH3-positive cardiomyocytes in AAV9-*Sav*-shRNA–injected hearts than in control hearts, indicating that cardiomyocytes were still cycling through M phase 3 months after viral injections ($P = 0.05$ and $P = 0.0123$ for GFP control compared to low-dose or high-dose *Sav*-shRNA, respectively; Fig. 4, E and F). For all of these proliferative indices, although there was a difference when AAV9-*Sav*-shRNA–injected groups were compared to controls, direct comparison of high- and low-dose AAV9-*Sav*-shRNA groups failed to show a difference.

To obtain further evidence that cardiomyocytes progressed through cytokinesis and divided, we performed immunofluorescence staining to monitor Aurora kinase B in the midbody remnant between divided cardiomyocytes. We often detected midbody Aurora kinase B staining between two divided cardiomyocytes in low-dose AAV9-*Sav*-shRNA–injected hearts but not in control hearts (Fig. 4, G and H). The number of Aurora kinase B–positive cardiomyocytes was higher at 45 days after myocardial infarction (pig age at euthanasia, 159 ± 12 days) than at 104 days after myocardial infarction (pig age at euthanasia, 190 ± 12 days), indicating that cardiomyocyte cell division was less frequent as cardiomyocytes repaired the tissue defect ($P < 0.0001$ and $P = 0.0041$ at 45 and 104 days after myocardial infarction, respectively; Fig. 4H). This finding is consistent with our previous observations in *Sav* loss-of-function mice, revealing that cell cycle entry was diminished at later stages of the heart repair process (12).

Because cardiomyocyte division should result in an increased number of mononucleated cells, we measured cardiomyocyte ploidy in pig cardiomyocytes (17, 33). The number of mononucleated cardiomyocytes in GFP-positive areas was higher in AAV9-*Sav*-shRNA–injected hearts than in control hearts ($P < 0.0001$; Fig. 5, A and B), providing further support that cardiomyocytes were dividing in AAV9-*Sav*-shRNA–injected hearts (pig age at euthanasia, 190 ± 12 days). Moreover, we counted cardiomyocyte numbers in GFP-positive areas and observed a higher cardiomyocyte density in AAV9-*Sav*-shRNA–injected hearts than in control hearts ($P = 0.0488$; Fig. 5C). These findings suggest that AAV9-*Sav*-shRNA induces cardiomyocyte division, ultimately improving left ventricular systolic function in this pig model of myocardial infarction.

Viral vector delivery of *Sav*-shRNA promotes transient cardiomyocyte sarcomere breakdown in pig hearts

Before entering the cell cycle and dividing, cardiomyocytes are believed to dedifferentiate and break down their sarcomere structure to overcome the structural block to cell division (3, 17, 34). We performed immunofluorescence staining for pHH3 and the sarcomere marker α-actinin to examine sarcomere structure in cardiomyocytes that were undergoing cell division in control and AAV9-*Sav*-shRNA–injected pig hearts (pig age at euthanasia, 190 ± 12 days). We observed a strong up-regulation of pHH3-positive cardiomyocytes with evidence of sarcomere breakdown in AAV9-*Sav*-shRNA–injected pig hearts but not in control hearts, supporting the notion that cardiomyocytes of AAV9-*Sav*-shRNA–injected hearts underwent dedifferentiation ($P = 0.0013$ and $P = 0.0059$ for GFP control compared to low-dose or high-dose *Sav*-shRNA, respectively; Fig. 5, D and E, and figs. S10, A and B).

To determine whether sarcomere breakdown was evident in cardiomyocytes that had divided and were no longer undergoing cell division, we examined sarcomere structure in EdU-positive and pHH3-negative cardiomyocytes. These cardiomyocytes exhibited a fully mature sarcomere structure, supporting the notion that cardiomyocyte dedifferentiation was transient in AAV9-*Sav*-shRNA–injected hearts. Paired EdU-positive cardiomyocytes that were identified in hearts injected with AAV9-*Sav*-shRNA also had a fully mature sarcomere structure (Fig. 5F). Connexin 43 (CX43), a gap junction component expressed in the intercalated discs of cardiomyocytes, has an essential function in synchronized cardiomyocyte excitation-contraction coupling (35). In AAV9-*Sav*-shRNA–injected hearts, immunofluorescence staining revealed the presence of CX43 in junctions between paired EdU-positive cardiomyocytes and surrounding cardiomyocytes, suggesting electrical coupling between cardiomyocytes that had divided (Fig. 5G). Together, these results suggest that newly divided cardiomyocytes became coupled and integrated into the myocardium of AAV9-*Sav*-shRNA–injected hearts.

Viral vector delivery of *Sav*-shRNA promotes vascularity in pig hearts after myocardial infarction

To determine whether AAV9-*Sav*-shRNA injection promotes vascularity in pig hearts after myocardial infarction, we performed immunofluorescence staining for the endothelial marker isolectin B4. Tiled image analysis revealed more capillary formation in low-dose AAV9-*Sav*-shRNA–injected hearts than in control hearts ($P = 0.0159$; figs. S11, A and

B) (pig age at euthanasia, 190 ± 12 days). We also investigated inflammatory responses using immunofluorescence staining to determine the number of CD45-positive leukocytes in the border zone of hearts after myocardial infarction. Immunofluorescence staining for CD45 revealed no differences in the number of leukocytes in the border zone of AAV9-*Sav*-shRNA–injected hearts versus control hearts, most likely because of waning of immune response 3 months after myocardial infarction (figs. S11, C and D, and tables S4 and S5). Thus, our findings indicate that AAV9-*Sav*-shRNA injection promoted persistent capillary formation in pig hearts after myocardial infarction.

DISCUSSION

Chronic human diseases such as heart failure are difficult to treat, commonly lethal, and associated with an aging population. A characteristic of nonregenerative organs such as the heart is that the functional cell type, such as the heart cardiomyocyte, is highly specialized with a limited capacity for self-renewal. Similar cellular characteristics are found in the neurons of the central nervous system and sensory organs. In addition to studies in the heart, recent studies have revealed that Hippo pathway loss of function or Yap gain of function can induce differentiated cells of the retina and cochlea to acquire a more fetal-like cell state in mice, which promotes regeneration of the retina and hair cells of the cochlea (36–38). Our study reveals that tissue renewal therapy—the approach of inducing tissue renewal by inhibiting an endogenous pathway in poorly regenerative organs—is effective and safe in the translational context of a large-animal model.

The cardiovascular system of pigs has important similarities to humans; thus, our study is an important step toward translation. Here, we show that using gene therapy to knock down the Hippo pathway in pig cardiomyocytes has cardiovascular benefits in a pig model of myocardial infarction. Pig hearts injected with AAV9-*Sav*-shRNA showed evidence of newly generated cardiomyocytes, reduced fibrosis, and increased small blood vessels. Our study provides evidence that AAV9-mediated gene therapy is cardiomyocyte specific, as we did not detect the deleterious effects of Hippo pathway loss of function in noncardiomyocyte cells in the heart such as cardiac fibroblasts (39). Tumor formation was not detected in other organs during the 3-month follow-up period.

Our findings differ from those of a recent study in pigs in which overexpression of miR199a initially improved heart function after myocardial infarction, but an eventual demise of the pigs occurred 2 months after viral vector delivery, most likely due to arrhythmia (15). Studies in mice have also shown that overexpression of constitutively active Yap or microRNAs broadly in the heart can be deleterious (16, 17). We monitored the pigs for 3 months after viral vector delivery, which is 1 month longer than the miR199a study, and did not observe lethality. Important differences in study design most likely account for the differences observed between these studies. For example, we used NOGA electromechanical mapping to specifically target the border zone cardiomyocytes. Localized injection of the cell type of interest may be an important advantage over the methods used to deliver miR199a, which involved an open thoracotomy with viral injection to the border zone (determined by visual inspection) at the time of myocardial infarction.

MicroRNAs are also known to have hundreds of conserved target genes, and this number may increase when a microRNA is overexpressed, leading to excessive suppression of target genes and off-target effects (40). Thus, whereas miR199a targets some Hippo pathway genes, it also regulates many other genes (41). Moreover, studies in mice suggest that miR199a gain of function may have harmful effects on heart function (42). We used a cardiac troponin T promoter element that was predicted to provide more cardiomyocyte specificity than the CMV promoter used previously (15). In addition, the capsid subtype we used, AAV9, may be less infectious than AAV6, which was used to express miR199a, resulting in a more muted expression of *Sav*-shRNAs (15). Our AAV9-GFP data indicated patchy expression of the viral vector localized to needle tracks, suggesting low efficiency of AAV9 infection in some cardiomyocytes.

It has been unclear whether the Hippo pathway's inhibitory regulation of cardiomyocyte proliferation is conserved in large mammals. Our functional data indicate that the Hippo pathway inhibits cardiomyocyte proliferation in pigs, suggesting that a similar effect would occur in the human heart. Consistent with observations in mice, we found in pigs that AAV9-*Sav*-shRNA treatment after myocardial infarction resulted in reduced cardiac fibrosis and increased small blood vessel formation, providing evidence that after myocardial infarction, Hippo pathway functions are conserved from mice to pigs. These findings demonstrate that AAV9-*Sav*-shRNA treatment induced a steady improvement in heart function in a manner that was safe and effective for treatment of heart disease.

Our study has some limitations. We were unable to determine whether the viral vector dose had a consistent impact on functional outcomes, and more work is required to address this question. In addition, it is known that humans are commonly exposed to AAVs and may have neutralizing antibodies (43, 44). Our study did not address the impact of neutralizing antibodies upon AAV9-*Sav*-shRNA treatment, and further study is required to address this important consideration. In addition, human cardiomyocytes are mostly mononucleated (45), whereas pig cardiomyocytes can have up to 16 nuclei (29). Given that polyploid cardiomyocytes have reduced proliferative and regenerative potential (46), determining how human cardiomyocytes respond to *Sav* knockdown with shRNA gene therapy will be an essential focus of future work.

MATERIALS AND METHODS

Study design

The objective of this study was to evaluate the therapeutic potential of Hippo pathway suppression in cardiomyocytes of a pig model of ischemic cardiomyopathy. AAV9-*Sav*-shRNA gene therapy was first tested in 3-month-old uninjured pig hearts and AAV9-GFP was used as the control. In a second experiment, myocardial infarction was induced by balloon angioplasty in 3-month-old domestic farm pigs. Two weeks after myocardial infarction, we used the NOGA mapping system to precisely deliver AAV9-*Sav*-shRNA ($n = 11$) or AAV9-GFP ($n = 7$) to the border zone of infarcted pig hearts. We followed the pigs for 3 months after AAV9 injection. Longitudinal heart functions were measured by echocardiography in 20- or 30-day intervals after viral injection (a total of six measurements). Cardiomyocyte proliferation was determined by EdU, pHH3, and Aurora

kinase B immunofluorescence staining. Pigs were grouped in a blinded and randomized fashion, and all investigators were blinded to the data. Statistical assumptions concerning the data, including normal distribution and similar variation between experimental groups, were examined for appropriateness before statistical tests were performed.

AAV9 viral packaging

Viral vectors were used as previously described (12). The construct containing triple shRNAs against *Sav* with flanking miR30 sequences was cloned into the pENN.AAV.cTNT, p1967-Q vector downstream of GFP (AAV9-*Sav*-shRNA). Empty vector–encoding GFP was used as the control (AAV9-GFP). Both vectors were packaged into the muscle-trophic serotype AAV9 by the Intellectual and Developmental Disabilities Research Center Neuroconnectivity Core at the Baylor College of Medicine. After titering, viruses were aliquoted (1×10^{13} viral genome particles per tube) and immediately frozen and placed at −80°C for long-term storage. Before each injection, each aliquot was diluted in saline to make a 3-ml injection solution.

Farm pigs

Farm pigs were handled and maintained in accordance with the requirements of the Laboratory Animal Welfare Act [Public Law (P.L.) 89-544] and its 1970 (P.L. 91-579), 1976 (P.L. 94-279), and 1985 (P.L. 99-198) amendments. Pigs were fed with a commercial diet and fresh clean water in a quantity sufficient to maintain body weight and permit reasonable weight gain in growing animals (table S6). Species-appropriate treats were given at the discretion of the attending veterinarian or designee.

When animals underwent surgery, they were given appropriate analgesic and antibiotic medications. Buprenorphine (0.05 to 0.1 mg/kg), administered intramuscularly or by mouth, was administered every 6 to 12 hours or as deemed necessary by the attending veterinarian. Flunixin meglumine (1.1 to 2.2 mg/kg) was administered intravenously, intramuscularly, or by mouth every 6 to 8 hours as needed. Naxcel (3 to 5 mg/kg) or the equivalent was administered intramuscularly once per day for 24 hours starting the day after the procedure. After Naxcel was discontinued, Baytril (enrofloxacin; 2.5 to 5.0 mg/kg) was administered by mouth twice per day for up to 7 days. Baytril [enrofloxacin; injectable solution, 7.5 mg/kg of body weight (3.4 ml/100 lbs)] was administered intramuscularly or subcutaneously (behind the ear). Continued use of antibiotics and analgesics was based on postprocedural monitoring unless otherwise specified. Nitroglycerin paste was applied topically after the myocardial infarction procedure, followed by aspirin [162.5 mg (one-half of a standard 325-mg tablet)] once per day by mouth and ranitidine (Zantac; 150 mg) 1 to 3 times per day by mouth. Last, pantoprazole (40 mg) was administered once per day by mouth for gastroprotection.

Electromechanical mapping and transendocardial injections

Electromechanical mapping was performed as previously described (47). Briefly, pigs were maintained on general anesthesia and were appropriately prepped and draped in a manner to allow sterile surgical access to the inguinal area. Femoral access was achieved by percutaneous penetration. An introducer sheath was positioned in the artery, and a MyoStar

injection catheter (Biosense Webster, Diamond Bar, CA, USA) was used to deliver AAV-*Sav*-shRNA or AAV-GFP. The catheter was advanced into the left ventricle to first create an electromechanical endocardial map. After the completion of point acquisition, the map was processed by using a moderate filter and a manual filter to exclude internal points, points taken outside the left ventricle cavity (e.g., atrial or aortic points), points acquired during premature ventricular contractions, or points that did not fulfill the standard quality criteria (e.g., loop stability > 6 mm, location stability > 4 mm, cycle length variation > 10%). After electromechanical mapping was completed, the MyoStar injection catheter was primed with 0.1 ml of AAV-*Sav*-shRNA or AAV-GFP to fill the dead space before the start of the injection procedure. The perpendicular positioning of the catheter into the left ventricle wall and the presence of a premature ventricular contraction upon extending the needle into the myocardium ensured proper delivery into the myocardium. For the pig model of myocardial infarction, the area of infarction was characterized with the NOGA system according to the presence of a low unipolar voltage (i.e., less than 4 mV). Border zones identified by electromechanical mapping are typically 5- to 10-mm regions adjacent to scar tissue (48). We performed 10 to 15 transendocardial injections to the border zone of the infarct (unipolar voltage value between 4 and 7 mV, 0.2 ml per injection). We then removed the catheter and closed the artery with Angio-Seal (Terumo). Pigs were then transferred to the intensive care unit for monitoring.

Acute myocardial infarction induced by I/R injury

We inserted a 6F sheet percutaneously in the common femoral artery. We advanced a 5F coronary guiding catheter through the aorta, and it was selectively engaged into the left main coronary ostium. Subsequently, an angioplasty balloon (chosen to match the left anterior ascending artery diameter) was positioned into the left anterior ascending artery between the first and second diagonal branch over a floppy 0.014-inch guidewire. The balloon was inflated at nominal pressure, and complete coronary occlusion was documented by the absence of the distal flow of contrast. After 90 min, the balloon was deflated, and passive reperfusion to the distal coronary bed was allowed. Patency of the distal circulation was documented by injecting contrast. Ventricular arrhythmias were prevented and treated with lidocaine (1.5-mg/kg boluses followed by continuous infusion), amiodarone (5-mg/kg boluses followed by continuous infusion), and electrical cardioversion, if necessary. During the coronary occlusion period, we periodically measured activated clotting time (ACT), and heparin boluses were repeated as needed to keep the ACT range between 250 and 350 s. After the procedure was completed, pigs were transferred to the intensive care unit for monitoring.

Two-dimensional echocardiography

Under general anesthesia, pigs were placed in the left lateral recumbent position. Oxygen saturation and 12-lead electrocardiograms were monitored. A 3.5-MHz phased-array transducer with a Vivid 7 ultrasound machine (GE Medical Systems, Milwaukee, WI, USA) was used to obtain images, including the parasternal long-axis view, parasternal short-axis view, and apex view. The left ventricle ejection fraction, left ventricle end-systolic volume, and left ventricle end-diastolic volume were calculated by using the biplane Simpson

method according to the guidelines of the American Society of Echocardiography (49). A blinded independent operator performed all analyses.

Pathologic report summary

Hearts and other organs (e.g., lungs, liver, and kidneys) were collected from 18 domestic pigs that underwent myocardial infarction and reperfusion 2 weeks before receiving transendocardial injections of AAV9-*Sav*-shRNA or AAV9-GFP virus. A total of 27 animals were included: 7 animals were euthanized at 45 days after myocardial infarction, 2 animals were euthanized at 74 days after myocardial infarction, and 18 animals were euthanized at 104 days after myocardial infarction (Table 1). Pigs with at least 30% ejection fraction reduction (relative to baseline) at 2 weeks after myocardial infarction were used for further experiments (50). We excluded two animals, P-1912 and P-1965, because of insufficient myocardial infarction induction. For P-1912, ejection fraction was 61% before myocardial infarction and 44% after myocardial infarction (a 28% reduction relative to baseline). For P-1965, ejection fraction was 54% before myocardial infarction and 38% after myocardial infarction (a 29% reduction relative to baseline).

One animal, P-1946, died shortly after receiving transendocardial injections. Examination of the heart revealed a large healing myocardial infarction in the anterior/anteroseptal left ventricle walls, from the apical to mid ventricular level. In addition, NOGA-injected sections showed two to three small foci of myocardial hemorrhage near the infarct border (fig. S4C). These foci were suggestive of acute injection sites and correlated with sites in the respective two-dimensional NOGA map.

Hearts from all other pigs showed gross and microscopic findings of focal replacement fibrosis that were compatible with a healed myocardial infarction of the left anterior ascending territory. All infarcted hearts showed typical left ventricle remodeling, with marked wall thinning in the involved territory (infarct size estimates are provided in Table 2). In a few of the pigs, smaller linear or patchy areas of fibrosis away from ischemic scar were considered procedure-related and were suggestive of healed injection sites or partial needle tracks.

In addition, small foci of interstitial or perivascular chronic inflammatory infiltrates were observed in 14 of the 18 pigs that were euthanized at 74 or 104 days after myocardial infarction (table S5). In most of these cases (11 of 14 affected), this finding was either mild or minimal and was occasionally associated with a single or small group of necrotic or vacuolated cardiomyocytes. However, in three animals, these areas were somewhat more extensive and diffuse (P-1895 and P-1918) or showed greater inflammation and myocyte loss with associated interstitial replacement fibrosis (P-1917). The infiltrated areas were present mostly in NOGA-injected sections. Inflammation score results are summarized in tables S4 and S5.

Gross findings in other organs were few and considered incidental or secondary to procedural manipulation. Lungs, liver, and kidneys collected at the time of euthanasia appeared mostly normal upon gross inspection. The lungs had various amounts of dark red discoloration, typically in the dorsal caudal aspect, which were generally attributed

to atelectasis due to dorsal recumbency, general anesthesia, and euthanasia. The kidneys had few incidental congenital findings consisting of severe renal hypoplasia (P-1864) and renal cysts (P-1903 and P-1947). The livers appeared unremarkable, with only one animal (P-1937) having thinning of the gallbladder wall (table S1).

A subset of pigs was selected for a limited microscopic examination of lung and liver tissues. The subset included nine animals: seven study pigs (P-1937, P-1947, P-1949, P-1950, P-1953, P-1956, and P-1960) mixed from both study arms and an untreated control pig (P-1989). Histologic sections from the middle regions of the respective organ were randomly selected and stained with hematoxylin and eosin (H&E). In all pigs except for one, the lungs showed no clinical findings other than some areas of atelectasis that are commonly attributed to the various procedures performed before euthanasia (general anesthesia and dorsal recumbency). One pig, P-1950, had focal interstitial pneumonia in its middle lobes, most likely related to the aspiration of foreign material. No clinical findings were observed in the liver, except for minimal focal inflammatory cell aggregates in one animal, P-1960. These findings are considered incidental (tables S1 to S3).

Heart sample processing

At the time of euthanization, hearts were excised, weighed, and photographed. After gross evaluation of the exterior, a fresh small sample was taken for cryosectioning and subsequent molecular analysis. Hearts were then perfusion fixed with 10% neutral-buffered formalin retrograde from the ascending aorta at about 100 mmHg pressure for 20 min. After perfusion-fixation, hearts were sliced according to a segmentation protocol designed for the sampling of hearts that underwent transendocardial injection with biologic agents (28). Heart slices and base were then immersed in 10% neutral-buffered formalin for 24 to 48 hours. Sections that had received the highest number of injections [as per the respective two-dimensional electromechanical mapping (NOGA) maps] were selected for analysis. Those sections were additionally sliced into four to five 2-mm-thick sections and embedded in different paraffin blocks (usually 40 to 50 blocks per heart). One to three additional samples from remote noninjected sections were also collected. All samples were processed for paraffin embedding, cut at 5-μm thickness, and stained with H&E.

Infarct size calculation

Ventricles were sectioned from apex to base into seven to eight transverse slices. Each slice was photographed on its apical and basal face. ImagePro software was used to analyze the digital images. Left ventricle and infarct areas were manually traced with ImagePro software from the digital photographs of the apical and basal faces of each slice. For each slice face, the infarct was calculated as a percentage of the left ventricle. The results of both faces were then averaged and multiplied by the slice weight to calculate the size of the infarct. The sum of the infarct sizes from all slices was then divided by the sum of the left ventricle weight from all slices and expressed as a percentage (51).

Immunofluorescence staining

Processed frozen and paraffin sections were used for downstream analyses. For frozen sections, after fixation, hearts were dehydrated in 15 and 30% sucrose gradients and

then embedded into optimal cutting temperature compound (catalog no. 25608-930, VWR International, Radnor, PA, USA) for sectioning. Slides were sectioned at 10-μm intervals for immunofluorescence staining. For paraffin sections, samples were deparaffinized and rehydrated, treated with 3% H_2O_2 in EtOH, treated with antigen retrieval solution (Vector Laboratories Inc., Burlingame, CA, USA), blocked with 10% donkey serum in phosphate-buffered saline, and then incubated with primary antibodies. Antibodies were as follows: goat anti-GFP (ab6673, Abcam, Cambridge, UK), rabbit anti-Yap (NB110-58358, Novus Biologicals, Littleton, CO, USA), rat anti-pHH3 (ab10543, Abcam), rabbit antisarcomeric actinin (ab9465, Abcam), mouse anti-CX43 (sc-13558, Santa Cruz Biotechnology Inc., Dallas, TX, USA), rabbit anti-CD45 (Abcam ab10559), rabbit anti-Aurora kinase B (Abcam ab2254), and isolectin B4 (FL-1201, Vector Laboratories).

EdU incorporation assay

EdU incorporation was detected by using the Click-it EdU Imaging Kit (Life Technologies, Carlsbad, CA, USA). Imaging of tissue slides was performed with a Leica TCS SP5 confocal microscope, and images were processed by using Leica LAS AF software (Leica Microsystems, Wetzlar, Germany).

Tile imaging analysis and machine learning

After immunofluorescence staining, tile images were captured by using a Zeiss LSM 880 with an Airyscan FAST Confocal Microscope at the Optical Imaging and Vital Microscopy Core of the Baylor College of Medicine. Each tile image includes at least $8 \times 8 = 64$ scan field at 10× objective-scanned images with 20% overlap for stitching (20 to 30 mm^2 per image). Images were then analyzed by Fiji (31) for machine learning. Pixel-based segmentation of images was produced with the plugin of Trainable Weka Segmentation (30), and the binary classifications whose area was larger than 300 pixels were added to regions of interest (ROIs) in Fiji. 4′,6-Diamidino-2-phenylindole staining in an area larger than 100 pixels was counted as nuclei, and the overlap between nuclei and ROIs was detected by Speckle Inspector and counted as one cell (52). We then filtered out cells in which nuclei were attached to the cell boundary (noncardiomyocytes; see fig. S3) by using intensity analysis on the updated ROI. Last, cardiomyocytes that overlapped with EdU staining were counted as EdU-positive cardiomyocytes.

Statistics

Throughout the study, all analyses were performed in a double-blinded manner. Data are presented as the means ± SEM. Quantitative data for two groups were statistically evaluated using the Mann-Whitney U test or the two-tailed paired t test. Normality was tested by quantile-quantile plot and Shapiro-Wilk test. For comparisons among multiple groups, we used two-way analysis of variance (ANOVA) with Bonferroni's pairwise post hoc test. A P value of less than 0.05 was considered significant for all analyses ($P < 0.05$). Significant differences between experimental groups were denoted as $*P < 0.05$, $**P < 0.01$, or $***P < 0.001$.

In these experiments, we were interested in how treatment altered a cardiomyocyte's ability to enter the cell cycle. Each animal received treatment as multiple discrete injections into

the left ventricle of the heart. We mapped/tracked where the injections were done using a physical (NOGA) map and a GFP reporter to show cells infected by the virus. Each injection site served as an island of infected cells surrounded by uninfected cells in between. We collected histology sections from injection locations for analysis (not an equal number from each animal due to limitations of sample availability and histology preparations). Each section had a measurement value. Because we could define each injection site and track cells that were infected with the viral vector, we categorized each tile image/section, rather than each pig, as the replicate. We displayed data in a nested graph format while keeping individual tile image/section as replicates in the nested figure and used ANOVA with posttesting to assess the effect of AAV9-*Sav*-shRNA treatment on the cardiomyocytes' ability to enter the cell cycle. We performed these analyses using GraphPad Prism software. For the ANOVA analysis, the assumption of independence was tested using the χ^2 test, normality was tested using a normal quantile-quantile plot, and equality of variance was tested using the Brown-Forsythe test or Bartlett's test. If the tests indicated that the homogeneity of variances assumption was invalid, we used the nonparametric Kruskall-Wallis ANOVA test.

Supplementary Material

Refer to Web version on PubMed Central for supplementary material.

Acknowledgments:

This work is dedicated to the memory of J.T.W., mentor, friend, and inspiration. We thank the Developmental Disabilities Research Center Neuroconnectivity Core at the Baylor College of Medicine for AAV9 viral vector and D. Vela of the Cardiovascular Pathology Research Department at the Texas Heart Institute for pathological analysis. We also thank the Data to Knowledge Lab at the Rice University and P. Safavi-Naeini at Texas Heart Institute for valuable consultation regarding our statistical analysis. N. Stancel of the Texas Heart Institute provided editorial support.

Funding:

This study was supported by grants from the NIH (HL 127717, HL 130804, and HL 118761 to J.F.M.), the Vivian L. Smith Foundation (J.F.M.), and Brown Foundation and State of Texas Funding (J.F.M. and J.T.W.). J.F.M. was supported by the LeDucq Foundation's Transatlantic Networks of Excellence in Cardiovascular Research (14CVD01 to J.F.M.), the MacDonald Research Fund Award (16RDM001 to J.F.M.), a grant from the Saving Tiny Hearts Society (to J.F.M), and an American Heart Association Postdoctoral Fellowship (18POST34060186 to S.L.).

Data and materials availability:

All data associated with this study are present in the paper or the Supplementary Materials. The plasmids are available upon request to J.F.M. through a materials transfer agreement.

REFERENCES AND NOTES

1. Leach JP, Martin JF, Cardiomyocyte proliferation for therapeutic regeneration. Curr. Cardiol. Rep 20, 63 (2018). [PubMed: 29904823]
2. Fu X, Khalil H, Kanisicak O, Boyer JG, Vagnozzi RJ, Maliken BD, Sargent MA, Prasad V, Valiente-Alandi I, Blaxall BC, Molkentin JD, Specialized fibroblast differentiated states underlie scar formation in the infarcted mouse heart. J. Clin. Invest 128, 2127–2143 (2018). [PubMed: 29664017]

3. Tzahor E, Poss KD, Cardiac regeneration strategies: Staying young at heart. Science 356, 1035–1039 (2017). [PubMed: 28596337]
4. Bergmann O, Zdunek S, Felker A, Salehpour M, Alkass K, Bernard S, Sjostrom SL, Szewczykowska M, Jackowska T, dos Remedios C, Malm T, Andrä M, Jashari R, Nyengaard JR, Possnert G, Jovinge S, Druid H, Frisén J, Dynamics of cell generation and turnover in the human heart. Cell 161, 1566–1575 (2015). [PubMed: 26073943]
5. Senyo SE, Steinhauser ML, Pizzimenti CL, Yang VK, Cai L, Wang M, Wu TD, Guerquin-Kern JL, Lechene CP, Lee RT, Mammalian heart renewal by pre-existing cardiomyocytes. Nature 493, 433–436 (2013). [PubMed: 23222518]
6. Ali SR, Hippenmeyer S, Saadat LV, Luo L, Weissman IL, Ardehali R, Existing cardiomyocytes generate cardiomyocytes at a low rate after birth in mice. Proc. Natl. Acad. Sci. U.S.A 111, 8850–8855 (2014). [PubMed: 24876275]
7. Porrello ER, Mahmoud AI, Simpson E, Hill JA, Richardson JA, Olson EN, Sadek HA, Transient regenerative potential of the neonatal mouse heart. Science 331, 1078–1080 (2011). [PubMed: 21350179]
8. Ye L, D'Agostino G, Loo SJ, Wang CX, Su LP, Tan SH, Tee GZ, Pua CJ, Pena EM, Cheng RB, Chen WC, Abdurrachim D, Lalic J, Tan RS, Lee TH, Zhang JY, Cook SA, Early regenerative capacity in the porcine heart. Circulation 138, 2798–2808 (2018). [PubMed: 30030417]
9. Zhu W, Zhang E, Zhao M, Chong Z, Fan C, Tang Y, Hunter JD, Borovjagin AV, Walcott GP, Chen JY, Qin G, Zhang J, Regenerative potential of neonatal porcine hearts. Circulation 138, 2809–2816 (2018). [PubMed: 30030418]
10. Haubner BJ, Schneider J, Schweigmann U, Schuetz T, Dichtl W, Velik-Salchner C, Stein JI, Penninger JM, Functional recovery of a human neonatal heart after severe myocardial infarction. Circ. Res 118, 216–221 (2016). [PubMed: 26659640]
11. Martin JF, Perin EC, Willerson JT, Direct stimulation of cardiogenesis: A new paradigm for treating heart disease. Circ. Res 121, 13–15 (2017). [PubMed: 28642324]
12. Leach JP, Heallen T, Zhang M, Rahmani M, Morikawa Y, Hill MC, Segura A, Willerson JT, Martin JF, Hippo pathway deficiency reverses systolic heart failure after infarction. Nature 550, 260–264 (2017). [PubMed: 28976966]
13. Bassat E, Mutlak YE, Genzelinakh A, Shadrin IY, Baruch Umansky K, Yifa O, Kain D, Rajchman D, Leach J, Riabov Bassat D, Udi Y, Sarig R, Sagi I, Martin JF, Bursac N, Cohen S, Tzahor E, The extracellular matrix protein agrin promotes heart regeneration in mice. Nature 547, 179–184 (2017). [PubMed: 28581497]
14. Morikawa Y, Heallen T, Leach J, Xiao Y, Martin JF, Dystrophin-glycoprotein complex sequesters Yap to inhibit cardiomyocyte proliferation. Nature 547, 227–231 (2017). [PubMed: 28581498]
15. Gabisonia K, Prosdocimo G, Aquaro GD, Carlucci L, Zentilin L, Secco I, Ali H, Braga L, Gorgodze N, Bernini F, Burchielli S, Collesi C, Zandonà L, Sinagra G, Piacenti M, Zacchigna S, Bussani R, Recchia FA, Giacca M, MicroRNA therapy stimulates uncontrolled cardiac repair after myocardial infarction in pigs. Nature 569, 418–422 (2019). [PubMed: 31068698]
16. Tian Y, Liu Y, Wang T, Zhou N, Kong J, Chen L, Snitow M, Morley M, Li D, Petrenko N, Zhou S, Lu M, Gao E, Koch WJ, Stewart KM, Morrisey EE, A microRNA-Hippo pathway that promotes cardiomyocyte proliferation and cardiac regeneration in mice. Sci. Transl. Med 7, 279ra238 (2015).
17. Monroe TO, Hill MC, Morikawa Y, Leach JP, Heallen T, Cao S, Krijger PHL, de Laat W, Wehrens XHT, Rodney GG, Martin JF, YAP partially reprograms chromatin accessibility to directly induce adult cardiogenesis. Dev. Cell 48, 765–779.e7 (2019). [PubMed: 30773489]
18. Gyöngyösi M, Dib N, Diagnostic and prognostic value of 3D NOGA mapping in ischemic heart disease. Nat. Rev. Cardiol 8, 393–404 (2011). [PubMed: 21587214]
19. Wang J, Liu S, Heallen T, Martin JF, The Hippo pathway in the heart: Pivotal roles in development, disease, and regeneration. Nat. Rev. Cardiol 15, 672–684 (2018). [PubMed: 30111784]
20. Morikawa Y, Zhang M, Heallen T, Leach J, Tao G, Xiao Y, Bai Y, Li W, Willerson JT, Martin JF, Actin cytoskeletal remodeling with protrusion formation is essential for heart regeneration in Hippo-deficient mice. Sci. Signal 8, ra41 (2015). [PubMed: 25943351]

21. Heallen T, Morikawa Y, Leach J, Tao G, Willerson JT, Johnson RL, Martin JF, Hippo signaling impedes adult heart regeneration. Development 140, 4683–4690 (2013). [PubMed: 24255096]
22. Spannbauer A, Traxler D, Zlabinger K, Gugerell A, Winkler J, Mester-Tonczar J, Lukovic D, Müller C, Riesenhuber M, Pavo N, Gyöngyösi M, Large animal models of heart failure with reduced ejection fraction (HFrEF). Front. Cardiovasc. Med 6, 117 (2019). [PubMed: 31475161]
23. van der Velden J, Merkus D, Klarenbeek BR, James AT, Boontje NM, Dekkers DH, Stienen GJ, Lamers JM, Duncker DJ, Alterations in myofilament function contribute to left ventricular dysfunction in pigs early after myocardial infarction. Circ. Res 95, e85–e95 (2004). [PubMed: 15528471]
24. Milani-Nejad N, Janssen PM, Small and large animal models in cardiac contraction research: Advantages and disadvantages. Pharmacol. Ther 141, 235–249 (2014). [PubMed: 24140081]
25. Stubenitsky R, van der Weerd RW, Haitsma DB, Verdouw PD, Duncker DJ, Cardiovascular effects of the novel Ca^{2+} sensitiser EMD 57033 in pigs at rest and during treadmill exercise. Br. J. Pharmacol 122, 1257–1270 (1997). [PubMed: 9421271]
26. McCormick ME, Manduchi E, Witschey WRT, Gorman RC, Gorman JH III, Jiang Y-Z, Stoeckert CJ Jr., Barker AJ, Markl M, Davies PF, Integrated regional cardiac hemodynamic imaging and RNA sequencing reveal corresponding heterogeneity of ventricular wall shear stress and endocardial transcriptome. J. Am. Heart Assoc 5, e003170 (2016). [PubMed: 27091183]
27. Gyöngyösi M, Pavo N, Lukovic D, Zlabinger K, Spannbauer A, Traxler D, Goliasch G, Mandic L, Bergler-Klein J, Gugerell A, Jakab A, Szankai Z, Toth L, Garamvölgyi R, Maurer G, Jaisser F, Zannad F, Thum T, Bátkai S, Winkler J, Porcine model of progressive cardiac hypertrophy and fibrosis with secondary postcapillary pulmonary hypertension. J. Transl. Med 15, 202 (2017). [PubMed: 28985746]
28. Vela D, Gahremanpour A, Buja LM, Method for sectioning and sampling hearts for histologic evaluation after delivery of biological agents by transendocardial injection. Cardiovasc. Pathol 24, 304–309 (2015). [PubMed: 26002556]
29. Velayutham N, Alfieri CM, Agnew EJ, Riggs KW, Baker RS, Ponny SR, Zafar F, Yutzey KE, Cardiomyocyte cell cycling, maturation, and growth by multinucleation in postnatal swine. J. Mol. Cell. Cardiol 146, 95–108 (2020). [PubMed: 32710980]
30. Arganda-Carreras I, Kaynig V, Rueden C, Eliceiri KW, Schindelin J, Cardona A, Sebastian Seung H, Trainable Weka Segmentation: A machine learning tool for microscopy pixel classification. Bioinformatics 33, 2424–2426 (2017). [PubMed: 28369169]
31. Schindelin J, Arganda-Carreras I, Frise E, Kaynig V, Longair M, Pietzsch T, Preibisch S, Rueden C, Saalfeld S, Schmid B, Tinevez JY, White DJ, Hartenstein V, Eliceiri K, Tomancak P, Cardona A, Fiji: An open-source platform for biological-image analysis. Nat. Methods 9, 676–682 (2012). [PubMed: 22743772]
32. Soonpaa MH, Rubart M, Field LJ, Challenges measuring cardiomyocyte renewal. Biochim. Biophys. Acta 1833, 799–803 (2013). [PubMed: 23142641]
33. Gan P, Patterson M, Sucov HM, Cardiomyocyte polyploidy and implications for heart regeneration. Annu. Rev. Physiol 82, 45–61 (2020). [PubMed: 31585517]
34. Ahuja P, Perriard E, Perriard JC, Ehler E, Sequential myofibrillar breakdown accompanies mitotic division of mammalian cardiomyocytes. J. Cell Sci 117, 3295–3306 (2004). [PubMed: 15226401]
35. Laird DW, Syndromic and nonsyndromic disease-linked Cx43 mutations. FEBS Lett. 588, 1339–1348 (2014). [PubMed: 24434540]
36. Gnedeva K, Wang X, McGovern MM, Barton M, Tao L, Trecek T, Monroe TO, Llamas J, Makmura W, Martin JF, Groves AK, Warchol M, Segil N, Organ of Corti size is governed by Yap/Tead-mediated progenitor self-renewal. Proc. Natl. Acad. Sci. U.S.A 117, 13552–13561 (2020). [PubMed: 32482884]
37. Rueda EM, Hall BM, Hill MC, Swinton PG, Tong X, Martin JF, Poché RA, The Hippo pathway blocks mammalian retinal muller glial cell reprogramming. Cell Rep. 27, 1637–1649.e6 (2019). [PubMed: 31067451]
38. Hamon A, García-García D, Ail D, Bitard J, Chesneau A, Dalkara D, Locker M, Roger JE, Perron M, Linking YAP to Muller glia quiescence exit in the degenerative retina. Cell Rep. 27, 1712–1725.e6 (2019). [PubMed: 31067458]

39. Xiao Y, Hill MC, Li L, Deshmukh V, Martin TJ, Wang J, Martin JF, Hippo pathway deletion in adult resting cardiac fibroblasts initiates a cell state transition with spontaneous and self-sustaining fibrosis. Genes Dev. 33, 1491–1505 (2019). [PubMed: 31558567]
40. Bartel DP, MicroRNAs: Target recognition and regulatory functions. Cell 136, 215–233 (2009). [PubMed: 19167326]
41. Torrini C, Cubero RJ, Dirkx E, Braga L, Ali H, Prosdocimo G, Gutierrez MI, Collesi C, Licastro D, Zentilin L, Mano M, Zacchigna S, Vendruscolo M, Marsili M, Samal A, Giacca M, Common regulatory pathways mediate activity of MicroRNAs inducing cardiomyocyte proliferation. Cell Rep. 27, 2759–2771.e5 (2019). [PubMed: 31141697]
42. el Azzouzi H, Leptidis S, Dirkx E, Hoeks J, van Bree B, Brand K, McClellan E, Poels E, Sluimer JC, van den Hoogenhof M, Armand AS, Yin X, Langley S, Bourajjaj M, Olieslagers S, Krishnan J, Vooijs M, Kurihara H, Stubbs A, Pinto YM, Krek W, Mayr M, da Costa Martins PA, Schrauwen P, de Windt LJ, The hypoxia-inducible microRNA cluster miR-199a~214 targets myocardial PPARδ and impairs mitochondrial fatty acid oxidation. Cell Metab. 18, 341–354 (2013). [PubMed: 24011070]
43. Louis Jeune V, Joergensen JA, Hajjar RJ, Weber T, Pre-existing anti–adeno-associated virus antibodies as a challenge in AAV gene therapy. Hum. Gene. Ther. Methods 24, 59–67 (2013). [PubMed: 23442094]
44. Vandamme C, Adjali O, Mingozzi F, Unraveling the complex story of immune responses to AAV vectors trial after trial. Hum. Gene Ther 28, 1061–1074 (2017). [PubMed: 28835127]
45. Olivetti G, Cigola E, Maestri R, Corradi D, Lagrasta C, Gambert SR, Anversa P, Aging, cardiac hypertrophy, and ischemic cardiomyopathy do not affect the proportion of mononucleated and multinucleated myocytes in the human heart. J. Mol. Cell. Cardiol 28, 1463–1477 (1996). [PubMed: 8841934]
46. González-Rosa JM, Sharpe M, Field D, Soonpaa MH, Field LJ, Burns CE, Burns CG, Myocardial polyploidization creates a barrier to heart regeneration in zebrafish. Dev. Cell 44, 433–446.e7 (2018). [PubMed: 29486195]
47. Vale PR, Losordo DW, Milliken CE, Maysky M, Esakof DD, Symes JF, Isner JM, Left ventricular electromechanical mapping to assess efficacy of phVEGF(165) gene transfer for therapeutic angiogenesis in chronic myocardial ischemia. Circulation 102, 965–974 (2000). [PubMed: 10961959]
48. Bolli R, Hare JM, March KL, Pepine CJ, Willerson JT, Perin EC, Yang PC, Henry TD, Traverse JH, Mitrani RD, Khan A, Hernandez-Schulman I, Taylor DA, DiFede D, Lima JAC, Chugh A, Loughran J, Vojvodic RW, Sayre SL, Bettencourt J, Cohen M, Moyé L, Ebert RF, Simari RD; Cardiovascular Cell Therapy Research Network (CCTRN), Rationale and design of the CONCERT-HF trial (combination of mesenchymal and c-kit(+) cardiac stem cells as regenerative therapy for heart failure). Circ. Res 122, 1703–1715 (2018). [PubMed: 29703749]
49. Lang RM, Badano LP, Mor-Avi V, Afilalo J, Armstrong A, Ernande L, Flachskampf FA, Foster E, Goldstein SA, Kuznetsova T, Lancellotti P, Muraru D, Picard MH, Rietzschel ER, Rudski L, Spencer KT, Tsang W, Voigt J-U, Recommendations for cardiac chamber quantification by echocardiography in adults: An update from the American Society of Echocardiography and the European Association of Cardiovascular Imaging. J. Am. Soc. Echocardiogr 28, 1–39.e14 (2015). [PubMed: 25559473]
50. Koudstaal S, Lorkeers SJ, Gho JMIH, van Hout GPJ, Jansen MS, Gründeman PF, Pasterkamp G, Doevendans PA, Hoefer IE, Chamuleau SAJ, Myocardial infarction and functional outcome assessment in pigs. J. Vis. Exp 2014, 51269 (2014).
51. Jones SP, Tang XL, Guo Y, Steenbergen C, Lefer DJ, Kukreja RC, Kong M, Li Q, Bhushan S, Zhu X, du J, Nong Y, Stowers HL, Kondo K, Hunt GN, Goodchild TT, Orr A, Chang CC, Ockaili R, Salloum FN, Bolli R, The NHLBI-sponsored Consortium for Preclinical Assessment of Cardioprotective therapies (CAESAR): A new paradigm for rigorous, accurate, and reproducible evaluation of putative infarct-sparing interventions in mice, rabbits, and pigs. Circ. Res 116, 572–586 (2015). [PubMed: 25499773]
52. Brocher J, Qualitative and quantitative evaluation of two new histogram limiting binarization algorithms. Int. J. Image Process 8, 30–48 (2014).

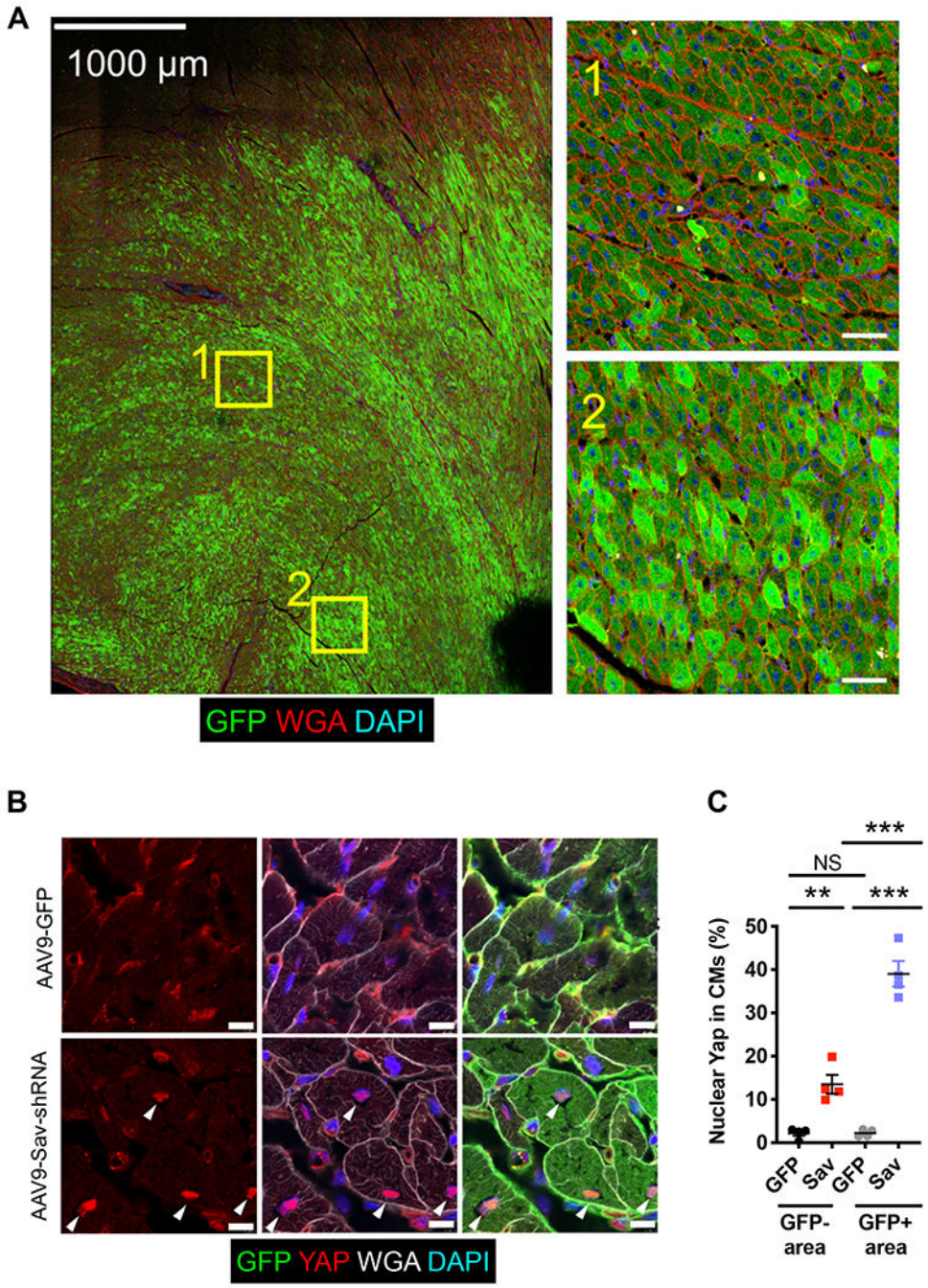

Fig. 1. Increased Yap nuclear localization in cardiomyocytes after AAV9-*Sav*-shRNA gene therapy.

(**A**) Shown is a representative tiled image of GFP staining of a section from an AAV9-*Sav*-shRNA–injected pig heart (pig P-1902; euthanized at 104 days and myocardial infarction, 33 days after viral vector injection). Inset images on the right show the magnification of the boxed areas in the tile image on the left. Scale bars, 1000 μm (left image) and 50 μm (right inset images). DAPI, 4′,6-diamidino-2-phenylindole. (**B**) Immunofluorescence staining for endogenous GFP and Yap shows the subcellular localization of Yap in GFP-

positive cardiomyocytes that received AAV9-*Sav*-shRNA gene therapy. White arrowheads indicate nuclear Yap. Scale bars, 10 μm. (**C**) Quantification of the percentage of nuclear Yap in GFP-positive and GFP-negative cardiomyocytes of pig hearts injected with AAV9-*Sav*-shRNA (Sav) or AAV9-GFP (GFP) as control ($n = 4$ per group). Data were compared using one-way ANOVA with Tukey's post hoc test. Data are presented as the mean ± SEM. $^{**}P < 0.01$ and $^{***}P < 0.001$; NS, not significant.

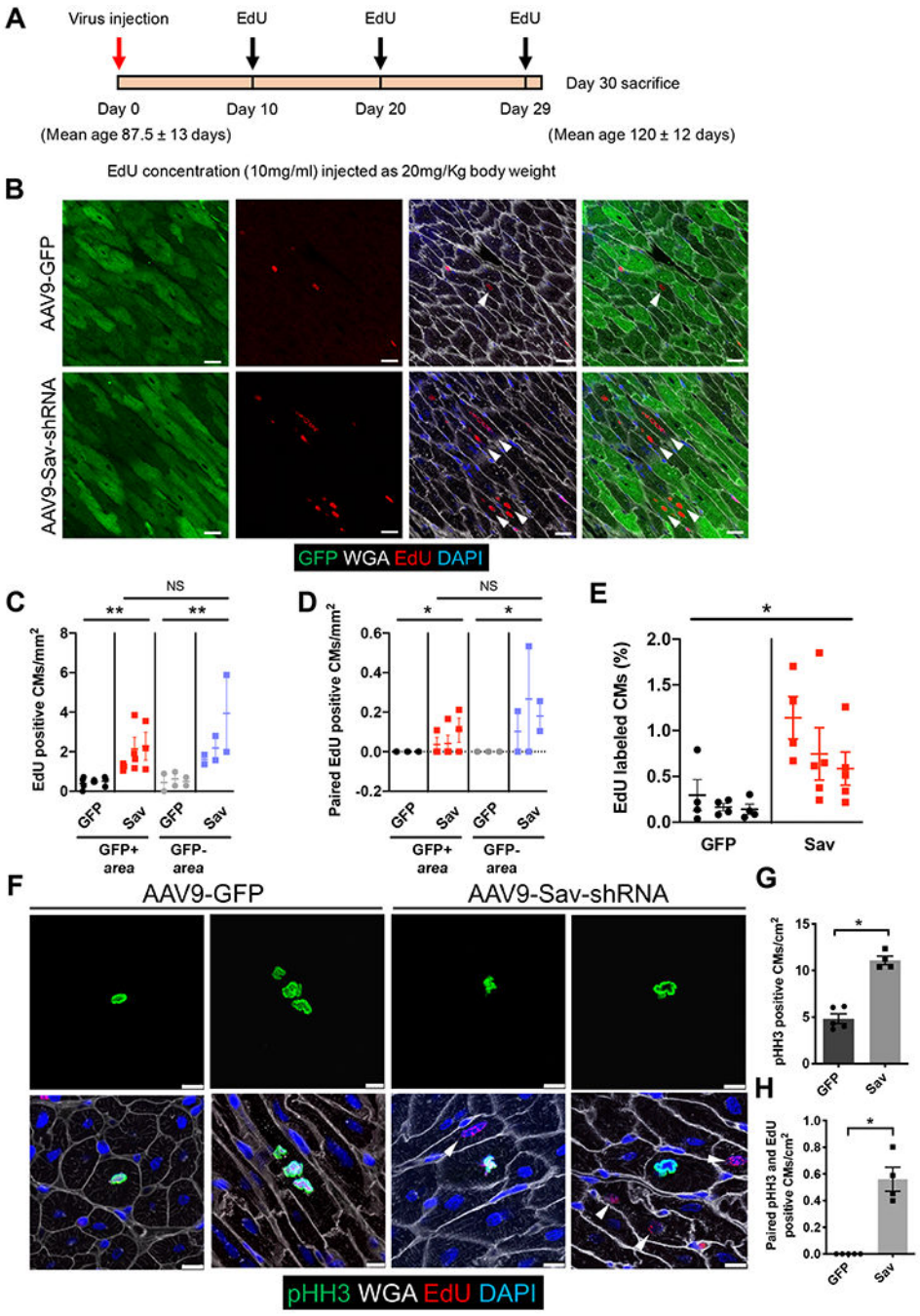

Fig. 2. Increased cardiomyocyte proliferation in uninjured pig hearts injected with AAV9-*Sav*-shRNA.

(**A**) Schematic shows the timing of viral vector and EdU injections. (**B**) Shown are representative images of immunofluorescence staining for GFP and EdU in the hearts of uninjured pigs (P-1890, AAV9-GFP control; P-1891, AAV9-*Sav*-shRNA). Both pigs were euthanized at the age of 120 days, 31 days after viral vector injection. White arrowheads indicate EdU-positive cardiomyocytes. Scale bars, 25 μm. (**C** and **D**) Shown is quantification of EdU-positive cardiomyocytes (C) and paired EdU-positive cardiomyocytes (D). Each

dot represents one tiled image ($n = 3$ per group). One-way ANOVA with Tukey's post hoc test was used for comparisons shown in (C); a nested *t* test was used for (D). (**E**) Machine learning quantification of EdU-positive cardiomyocytes is shown ($n = 3$). Four to five tiled images were analyzed per pig heart. A nested *t* test was used for the comparison. (**F**) Representative images show immunofluorescence staining for pHH3 and EdU in pig hearts (P-1900, AAV9-GFP control; P1902, AAV9-*Sav*-shRNA). White arrowheads indicate EdU-positive cardiomyocytes near pHH3-positive cardiomyocytes. Scale bars, 10 μm. (**G**) Shown is quantification of the number of pHH3-positive cardiomyocytes: GFP control, 4.84 ± 0.524 cardiomyocytes per cm^2; AAV9-*Sav*-shRNA (Sav) 11.10 ± 0.460 cardiomyocytes per cm^2 (GFP, $n = 5$; Sav, $n = 4$). (**H**) Shown is quantification of the number of paired pHH3-positive and EdU-positive cardiomyocytes, that is, the number of pHH3-positive cardiomyocytes with adjacent EdU-positive cardiomyocytes (GFP control, $n = 5$; Sav, $n = 4$). The Mann-Whitney test was used for comparisons for (G) and (H). Data are presented as the means ± SEM. For all comparisons, $*P < 0.05$, $**P < 0.01$.

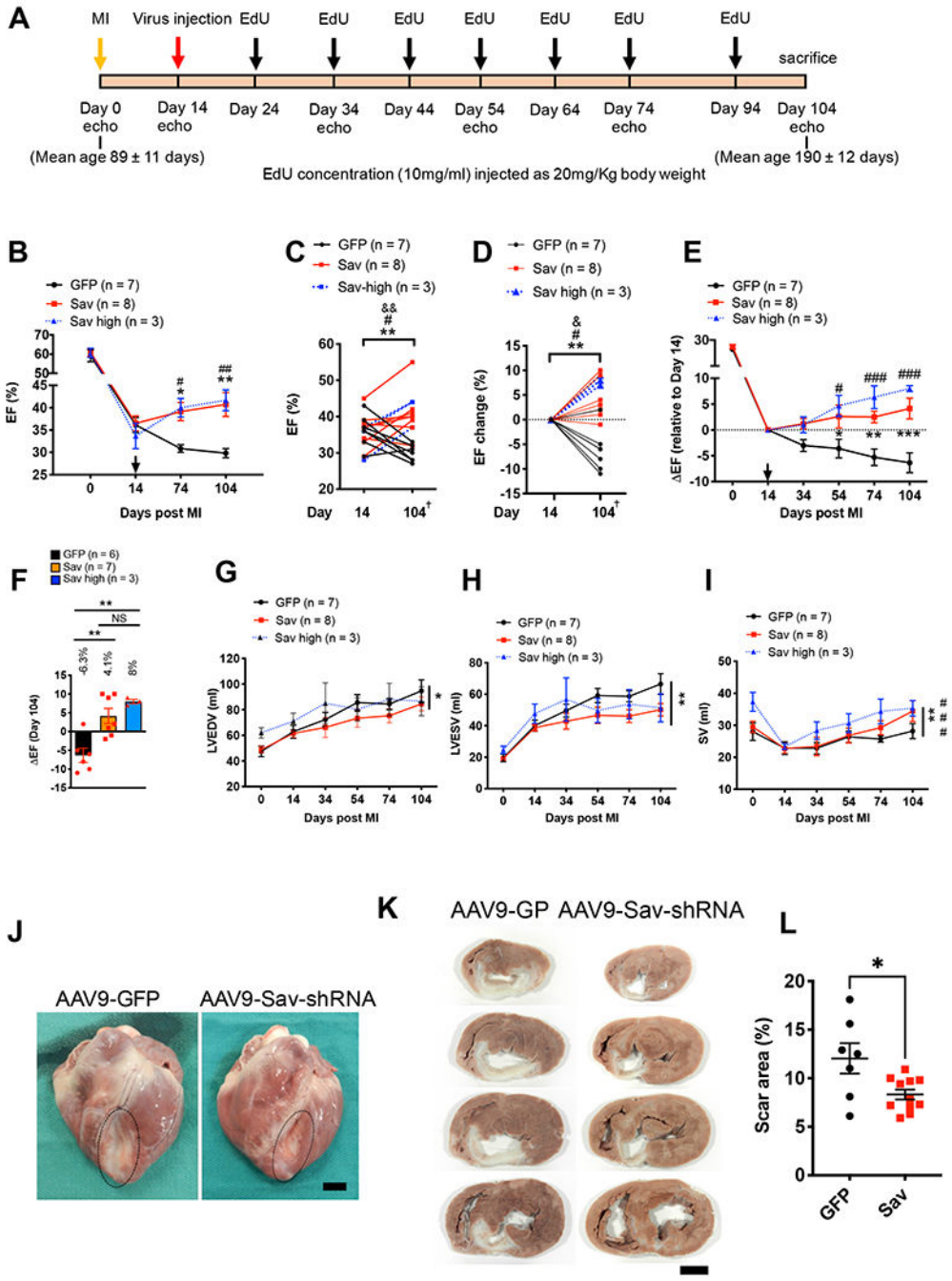

Fig. 3. Improved heart function in pigs with myocardial infarction after AAV9-*Sav*-shRNA gene therapy.

(**A**) Schematic shows the timing of viral vector injection, EdU injections, and echocardiography (echo) studies in a pig model of I/R-induced myocardial infarction (MI). (**B** to **D**) Echocardiography results show the ejection fraction (EF) after myocardial infarction (B), the ejection fraction at day 14 to 104 after myocardial infarction (C), and the change in ejection fraction from days 14 to 104 after myocardial infarction (D); Two-tailed paired *t* test was used in (C), and two-way ANOVA with Bonferroni post hoc test was

used in (D). *, #, and & indicate comparison between days 14 and 104 after myocardial infarction for AAV9-GFP control (GFP) pig heart and low- (Sav) and high-dose (Sav high) pig hearts injected with AAV9-*Sav*-shRNA respectively. * and &$P < 0.05$, **, ##, and &&$P < 0.01$; # = 0.07 in C, # = 0.0339 in D. arrow indicates virus injection in B; + indicates one pig treated with AAV9-GFP and one pig treated with low dose AAV9-Sav-shRNA that were both euthanized at day 74 post myocardial infarction. (**E** and **F**) Longitudinal plot of changes in EF associated with day 14 after myocardial infarction for AAV9-GFP control and low-dose (Sav) and high-dose (Sav high) AAV9-*Sav*-shRNA (E). Bar graph with individual data points shows changes in ejection fraction on day 104 relative to day 14 after myocardial infarction (F). (**G** to **I**) Shown are left ventricular end-diastolic volume (LVEDV) (G), left ventricular end-systolic volume (LVESV) (H), and stroke volume (SV) (I) for pigs treated with AAV9-GFP as control ($n = 7$), low-dose AAV9-*Sav*-shRNA (Sav; $n = 8$), or high-dose AAV9-*Sav*-shRNA (Sav high; $n = 3$) gene therapy. Two-way ANOVA with Bonferroni's post hoc test was used for comparisons in (B), (E), (G), (H), and (I); one-way ANOVA with Tukey's post hoc test was used for panel (F); Asterisk indicates comparison between AAV9-GFP (GFP) control and AAV9-*Sav*-shRNA low dose (Sav); # indicates the comparison between AAV9-GFP control and AAV9-*Sav*-shRNA high dose (Sav high). * or #$P < 0.05$, ** or ##$P < 0.01$, and *** or ###$P < 0.001$. B, E, G, H, and I include one pig treated with AAV9-GFP and one pig treated with low dose AAV9-Sav-shRNA that were both euthanized at day 74 post myocardial infarction. (**J**) Representative images show pig hearts that were harvested 90 days after viral vector injection (P-1918, AAV9-GFP control; P-1917, AAV9-*Sav*-shRNA). Each pig underwent myocardial infarction at the age of 92 days, received viral vector at the age of 106 days, and was euthanized at the age of 196 days. Scale bar, 2 cm. (**K**) Shown are four representative heart slices from a total of 7 slices (slice numbers 3, 4, 5, and 6) for pigs P-1918 (AAV9-GFP control) and P-1917 (AAV9-*Sav*-shRNA). Scale bar, 2 cm. (**L**) Shown is quantification of scar size (AAV9-GFP, $n = 7$; combined low- and high-dose AAV9-*Sav*-shRNA, $n = 11$). The Mann-Whitney test was used for the comparison. Data are presented as the means ± SEM. *$P < 0.05$.

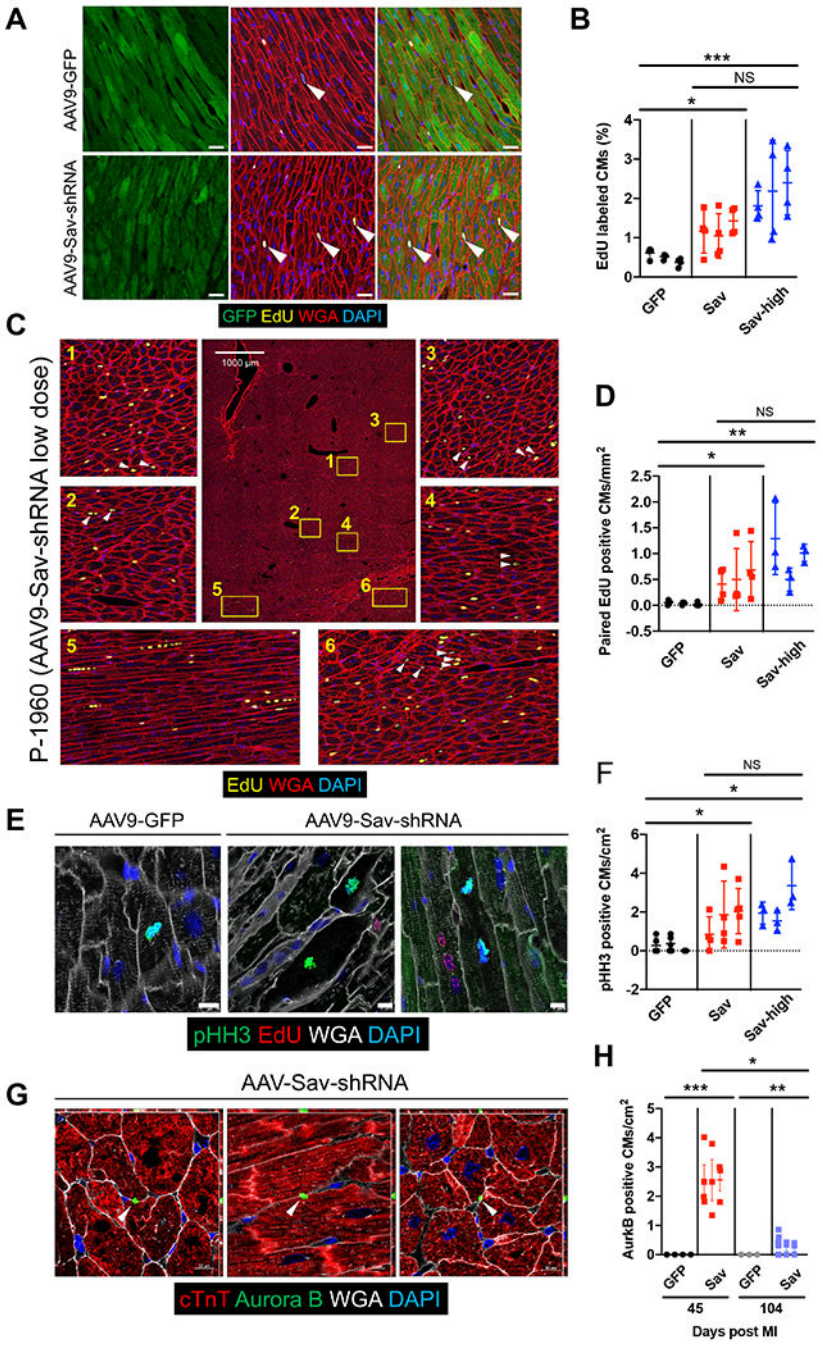

Fig. 4. Increased cardiomyocyte proliferation in pigs injected with AAV9-*Sav*-shRNA after myocardial infarction.

(**A**) Representative immunofluorescence images show EdU-positive cardiomyocytes (yellow) in the GFP-positive area (green) of heart sections from two pigs after myocardial infarction, one treated with AAV9-GFP (control) and the other treated with low-dose (Sav) AAV9-*Sav*-shRNA gene therapy. White arrowheads indicate EdU-positive cardiomyocytes. Scale bars, 25 μm. (**B**) Quantification of EdU-positive cardiomyocytes was determined via machine learning. For each pig, four tiled images were analyzed (n = 3 pigs per group).

(**C**) Representative tile image shows clustered EdU-positive cardiomyocytes in the heart of pig P-1960 (injected with low-dose AAV9-*Sav*-shRNA). White arrowheads indicate paired EdU-positive cardiomyocytes. (**D**) Quantification of paired EdU-positive cardiomyocytes (CMs) in the hearts of pigs receiving AAV9-GFP (control) or AAV9-*Sav*-shRNA gene therapy. For each pig, three to four tiled images were captured ($n = 3$ pigs per group). (**E**) Shown is immunofluorescence costaining for pHH3 and EdU in sections from pig hearts at 3 months after injection with AAV9-GFP (control) or low-dose AAV9-*Sav*-shRNA. Scale bars, 10 μm. (**F**) Quantification of pHH3-positive cardiomyocytes is presented. For each pig heart, three to five different sections were evaluated from each pig ($n = 3$). **(G)** Aurora kinase B staining in low-dose AAV9-*Sav*-shRNA–injected pig hearts 45 days after myocardial infarction. Quantification is shown in (**H**). Three to four heart sections were evaluated from each pig ($n = 4$ for GFP group at day 45 after myocardial infarction, $n = 3$ for other groups). White arrowhead indicates Aurora kinase B staining. In (B), (D), (F), and (H), GFP, Sav, and Sav-high groups indicate pig hearts injected with AAV9-GFP (control) or low- or high-dose AAV9-*Sav*-shRNA, respectively. ANOVA Kruskall-Wallis test with Dunn's multiple comparisons test were used in (B) and (H); nested *t* test was used to compare the difference between GFP and Sav 104 days after myocardial infarction in (H). Nested one-way ANOVA with Dunnett's post hoc test was used for comparisons shown in (D) and (F). Data are presented as the means ± SEM. $*P < 0.05$, $**P < 0.01$, and $***P < 0.001$.

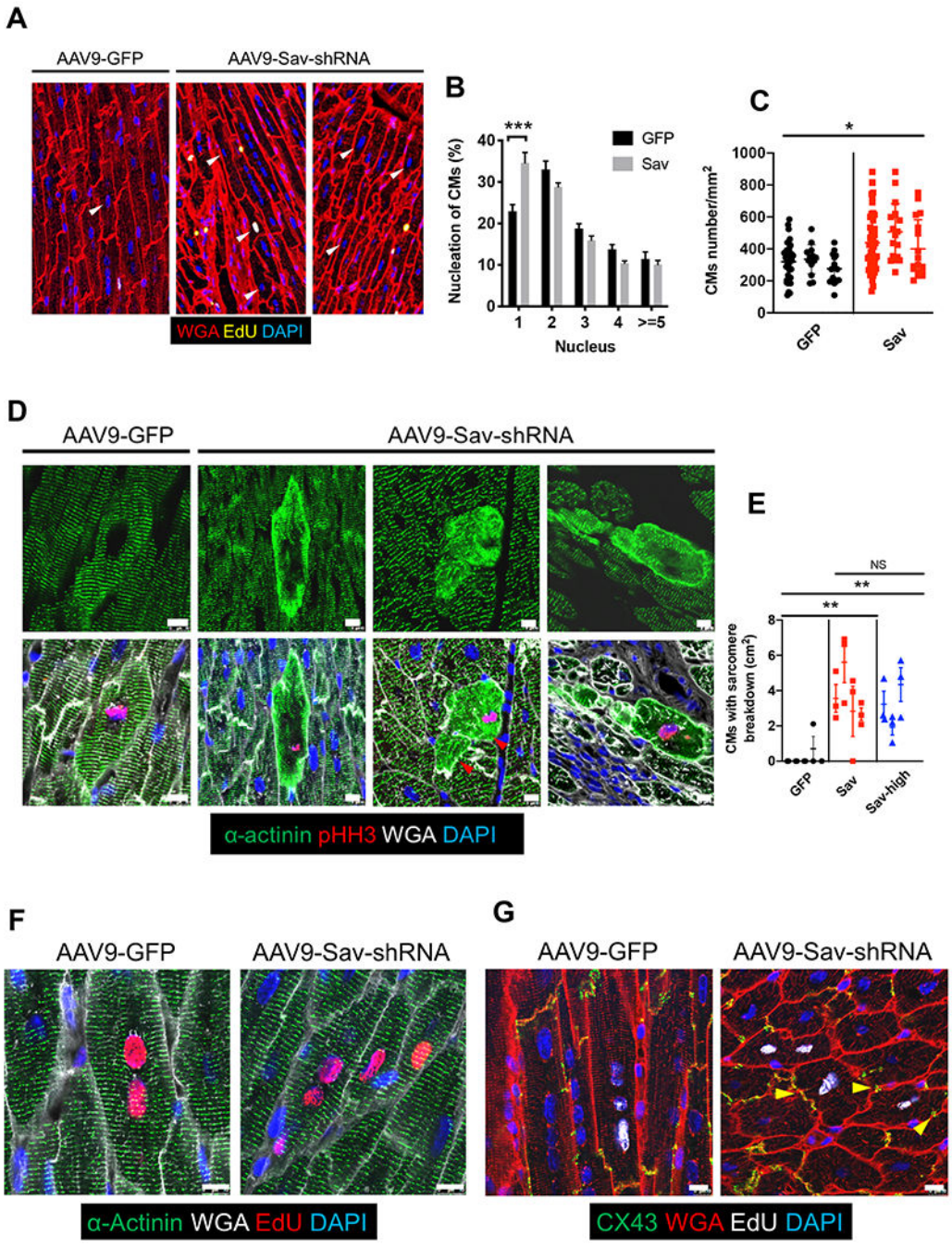

Fig. 5. Sarcomere breakdown and cardiomyocyte division in pigs injected with AAV9-*Sav*-shRNA after myocardial infarction.

(**A**) Shown is a representative image of a pig heart showing the number of nuclei in cardiomyocytes. White arrowheads indicate cardiomyocytes with one nucleus. (**B**) Shown is the percentage of cardiomyocytes with a different number of nuclei. For each pig, at least four tiled images were analyzed ($n = 4$). A total of 1327 cells were counted in the AAV9-GFP (GFP, control) group, and 1298 cells were counted in the high-dose AAV9-*Sav*-shRNA (Sav) group. ANOVA with Bonferroni's post hoc test was used for

comparisons. (**C**) Cardiomyocyte numbers in the GFP-positive area of a representative pig heart from each group are shown: AAV9-GFP control (GFP); AAV9-*Sav*-shRNA, low and high dose combined (Sav). Each dot represents counted cardiomyocytes in a GFP-positive area (normalized to mm^2) ($n = 3$). (**D**) Immunofluorescence stainings for pHH3 and sarcomere actinin are shown for representative sections from hearts in each group: AAV9-GFP control (GFP); low-dose AAV9-*Sav*-shRNA (Sav). Red arrowheads indicate dividing cardiomyocytes with sarcomere breakdown positioned side by side. Scale bars, 10 μm. (**E**) Shown is quantification of data in (D) ($n = 5$ for AAV9-GFP–injected hearts; $n = 4$ for low-dose AAV9-*Sav*-shRNA–injected hearts, and $n = 3$ for high-dose AAV9-*Sav*-shRNA–injected hearts). We quantified three different sections for each pig heart. Two-way ANOVA with Bonferroni's post hoc test was used for comparisons in (B); nested *t* tests were used for comparisons in (C); nested one-way ANOVA with Tukey's post hoc test were used for comparisons in (E). Data are presented as the means ± SEM. $*P < 0.05$, $**P < 0.01$, and $***P < 0.001$. (**F**) Shown is immunofluorescence staining for EdU and sarcomere actinin in cardiomyocytes from pig hearts injected with AAV9-GFP control or low-dose AAV9-*Sav*-shRNA. Coupled EdU-positive parent and daughter cardiomyocytes retain normal sarcomere structure after cell division in AAV9-*Sav*-shRNA–injected pig hearts. Scale bars, 10 μm. (**G**) Shown is immunofluorescence staining for EdU and connexin 43 (CX43) in cardiomyocytes from pig hearts injected with AAV9-GFP control or AAV9-*Sav*-shRNA. Coupled EdU-positive cardiomyocytes connect with each other via CX43 after cell division in AAV9-*Sav*-shRNA–injected pig hearts. Yellow arrowheads indicate CX43 staining. Scale bars, 25 μm.

Table 1.

Age and sex data for pigs in this study.

Protocol 2018-12 (Non–myocardial infarction)							
ID number	**Date of birth**	**Procedure date**	**Sex**	**Virus injected**	**Age at injection (days)**	**Date of euthanasia**	**Age at euthanasia (days)**
P-1890	4/26/2018	7/24/2018	Female	GFP	89	8/24/2018	120
P-1891	4/26/2018	7/24/2018	Male	Sav	89	8/24/2018	120
P-1900	6/20/2018	8/30/2018	Female	GFP	71	10/2/2018	104
P-1902	6/20/2018	8/30/2018	Female	Sav	71	10/2/2018	104
P-1905	6/20/2018	9/6/2018	Male	GFP	78	10/9/2018	111
P-1906	6/20/2018	9/6/2018	Male	Sav	78	10/9/2018	111
P-1913	7/18/2018	10/11/2018	Male	GFP	85	11/13/2018	118
P-1915	7/18/2018	10/11/2018	Male	Sav	85	11/13/2018	118
P-1921	7/18/2018	11/6/2018	Male	GFP	111	12/7/2018	142
P-1922	7/18/2018	11/6/2018	Male	Sav	111	12/7/2018	142
P-1932	8/16/2018	11/15/2018	Male	GFP	91	12/18/2018	124
P-1933	8/16/2018	11/15/2018	Male	Sav	91	12/18/2018	124

Protocol 2018-25 (Myocardial infarction)									
ID number	**Date of birth**	**Myocardial infarction induction date**	**Procedure date (viral injection)**	**Sex**	**Virus injected**	**Age at surgery (days)**	**Age at injection (days)**	**Date of euthanasia**	**Age at euthanasia (days)**
P-1894	4/30/2018	8/7/2018	8/21/2018	Female	GFP	99	113	10/23/2018	176
P-1895	4/30/2018	8/7/2018	8/21/2018	Female	Sav	99	113	10/23/2018	176
P-1896	5/23/2018	8/14/2018	8/28/2018	Male	GFP	83	97	11/27/2018	188
P-1897	5/23/2018	8/14/2018	8/28/2018	Male	Sav	83	97	11/27/2018	188
P-1903	6/20/2018	9/4/2018	9/18/2018	Male	Sav	76	90	12/17/2018	180
P-1917	7/18/2018	10/18/2018	11/1/2018	Male	Sav	92	106	1/30/2019	196
P-1918	7/18/2018	10/18/2018	11/1/2018	Male	GFP	92	106	1/30/2019	196
P-1937	9/20/2018	1/8/2019	1/22/2019	Male	Sav	111	125	4/22/2019	215
P-1947	11/7/2018	1/15/2019	1/31/2019	Male	GFP	69	85	5/2/2019	176
P-1949	10/26/2018	1/24/2019	2/7/2019	Female	GFP	90	104	5/9/2019	195

Protocol 2018-12 (Non–myocardial infarction)									
ID number	**Date of birth**	**Procedure date**	**Sex**	**Virus injected**	**Age at injection (days)**		**Date of euthanasia**		**Age at euthanasia (days)**
P-1950	11/7/2018	1/28/2019	2/11/2019	Female	GFP	82	96	5/13/2019	187
P-1953	11/7/2018	1/28/2019	2/11/2019	Female	Sav	82	96	5/13/2019	187
P-1956	11/7/2018	2/5/2019	2/19/2019	Female	Sav	90	104	5/20/2019	194
P-1960	12/6/2018	2/21/2019	3/7/2019	Female	Sav	77	91	6/5/2019	181
P-2019	7/7/2019	10/24/2019	11/7/2019	Male	Sav-high dose	109	123	2/6/2020	214
P-2020	7/2/2019	10/24/2019	11/7/2019	Male	GFP	114	128	2/6/2020	219
P-2022	7/2/2019	10/29/2019	11/14/2019	Male	Sav-high dose	121	135	2/13/2020	226
P-2053	1/27/2019	5/5/2020	5/21/2020	Male	Sav-high dose	98	114	8/17/2020	202
P-2066	4/18/2020	8/18/2020	9/3/2020	Male	Sav	122	138	10/2/2020	167
P-2067	4/17/2020	8/19/2020	9/3/2020	Male	GFP	124	139	10/2/2020	168
P-2069	6/9/2020	10/1/2020	10/15/2020	Male	GFP	114	128	11/13/2020	157
P-2070	6/9/2020	10/7/2020	10/22/2020	Male	GFP	120	135	11/20/2020	164
P-2071	6/1/2020	10/8/2020	10/22/2020	Male	Sav	129	143	11/20/2020	172
P-2073	8/17/2020	11/19/2020	12/1/2020	Male	GFP	94	124	1/5/2021	141
P-2075	8/14/2020	11/23/2020	12/8/2020	Male	Sav	101	116	1/8/2021	147

Number of pigs treated with gene therapy			
Euthanized at day 74	**Euthanized at day 104**	**Euthanized at day 45**	**Excluded**
2	16	7	2

Sci Transl Med. Author manuscript; available in PMC 2022 September 15.

Table 2.

Evaluation of infarct size.

Animal ID	Age at myocardial infarction	Infarct size
	(days)	% (Infarct/left ventricle)
P-1894	75	12.5
P-1895	75	10.9
P-1896	104	8.1
P-1897	104	7.1
P-1903	104	6.3
P-1917	104	9.8
P-1918	104	18.1
P-1964	15	24.1
P-1937	104	9.7
P-1947	104	11
P-1949	104	15.6
P-1950	104	12.9
P-1953	104	7.3
P-1956	104	7.9
P-1960	104	7.2
P-2019	104	10
P-2020	104	6.1
P-2022	104	5.9

Table 3.

Blood test results 45 days after viral vector injection.

AST (SGOT), aspartate aminotransferase (serum glutamic-oxaloacetic transaminase); ALT (SGPT), alanine aminotransferase (serum glutamic-pyruvic transaminase); GGT, gamma-glutamyltransferase; BUN, blood urea nitrogen; WBC, white blood cells; RBC, red blood cells; HGB, hemoglobin; HCT, hematocrit; MCV, mean corpuscular volume; MCH, mean corpuscular hemoglobin; MCHC, mean corpuscular hemoglobin concentration.

	AAV9-GFP					AAV9-*Sav*-shRNA					
Animal ID	**P-2020**	**P-1894**	**P-1896**	**Ave ± SEM**		**P-1895**	**P-1897**	**P-2019**	**P-2022**	**Ave ± SEM**	
Total protein	5.6	6	4.5	5.37 ± 0.45		5.8	4.7	5.2	5.4	5.28 ± 0.20	
Albumin	3	4.2	3.1	3.43 ± 0.38		3.5	3	3.1	2.9	3.13 ± 0.11	
AST (SGOT)	22	24	14	20 ± 3.06		14	15	28	22	19.75 ± 2.84	
ALT (SGPT)	66	62	47	58.33 ± 5.78		66	54	39	53	53 ± 4.78	
Alkaline phosphatase	96	127	154	125.67 ± 16.76		147	143	76	95	115.25 ± 15.27	
GGT	37	28	15	26.67 ± 6.39		31	25	35	23	28.5 ± 2.38	
Total bilirubin	0.1	0.2	0.3	0.20 ± 0.06		0.2	0.2	0.1	0.2	0.175 ± 0.02	
BUN	8	8.6	17.2	11.27 ± 2.97		8	14.1	11	12	11.28 ± 1.10	
Creatinine	1.5	1.6	1.6	1.57 ± 0.03		1.5	1.6	1.6	1.6	1.58 ± 0.02	
Phosphorus	7	7.5	7.7	7.40 ± 0.21	High	8.7	8.1	7.3	7.3	7.85 ± 0.29	High
Glucose	87	81.5	76.8	81.77 ± 2.95		93.4	78.1	64	39	68.63 ± 10.00	
Calcium	9.5	9.7	9.6	9.60 ± 0.06		9.5	9.5	8.8	8.6	9.1 ± 0.20	
Magnesium	1.7	2.1	2.4	2.07 ± 0.20		1.9	2.3	1.5	1.7	1.85 ± 0.15	
Sodium	142	136.9	139.5	139.47 ± 1.47		140.9	139.3	142	146	142.05 ± 1.24	
Potassium	4	4.2	3.9	4.03 ± 0.09		3.8	3.8	3.8	4.1	3.875 ± 0.06	
Chloride	101	96	98	98.33 ± 1.45	Low	98.2	98	99	100	98.8 ± 0.39	Low
Cholesterol	80	90	74	81.33 ± 4.67	Low	96	70	76	68	77.5 ± 5.54	Low
WBC	8.3	10.5	10.9	9.90 ± 0.81		12.9	12.8	10.5	7.4	10.9 ± 1.12	
RBC	5.5	6.04	4.5	5.35 ± 0.45		5.29	4.06	5.4	5.2	4.99 ± 0.27	
HGB	9.5	11.4	8.1	9.67 ± 0.96		9.2	8.4	9.7	8	8.83 ± 0.33	
HCT	30	33.1	22.5	28.53 ± 3.15		27.3	23.5	30	26	26.7 ± 1.17	
MCV	55	54.8	50	53.27 ± 1.63		51.6	57.8	55	49	53.35 ± 1.67	
MCH	17.4	18.9	18	18.10 ± 0.44		17.4	20.7	18	15.5	17.9 ± 0.93	

	AAV9-GFP					AAV9-*Sav*-shRNA					
Animal ID	**P-2020**	**P-1894**	**P-1896**	**Ave ± SEM**		**P-1895**	**P-1897**	**P-2019**	**P-2022**	**Ave ± SEM**	
MCHC	32	34.5	36	34.17 ± 1.17	High	33.7	35.8	33	31	33.38 ± 0.86	High
Platelet count	361	269	205	278.33 ± 45.27		440	289	306	461	374 ± 38.55	
Lymphocytes	69%	64%	75%	69% ± 3.2		66.70%	65.80%	70%	66%	67% ± 0.85	